DOI: 10.26599/FSHW.2026.9251181

Contents lists available at SciOpen

Food Science and Human Wellness

journal homepage: https://www.sciopen.com/journal/2097-0765

China Food Publishing Co.

Inhibition of Xanthine Oxidase by Dietary Flavonoids: SWISS-MODEL-Based Docking, *In Vitro* Analysis, *In Vivo* Structure-Activity Investigations and Gut Microbiota-Based Systematic Toxicological Evaluation

Pingping Guo[a,#], Xingxing Liu[a,#], Fengying Dong[a], Gangao Yang[a], Jinghan Jia[a], Xinhua Song[a], lingru Li[b], Wenlong Sun[a,*], Yanfei Zheng[b,*].

[a]*School of Life Sciences and Medicine, Shandong University of Technology, Zibo 255000, China.*

[b]*National Institute of TCM Constitution and Preventive Medicine, Beijing University of Chinese Medicine, Beijing 100000, China.*

ABSTRACT: Hyperuricemia (HUA), a prevalent metabolic disorder, needs new xanthine oxidase (XOD) inhibitor studies to reduce severe side effects. In this study, the inhibitory activities of 20 dietary flavonoids against XOD were determined *in vitro*, and a structure-activity relationship (SAR) model was subsequently developed. Diosmetin and quercetin emerged as the most potent inhibitors, both of which displayed mixed-type inhibition. SWISS-MODEL-based docking revealed that the key binding sites for diosmetin are Asn768 (active site) and Phe1009 (allosteric site), whereas those for quercetin are Lys771 (active site) and Phe914 (allosteric site). In hyperuricemic mice, diosmetin and quercetin reduced serum uric acid levels, suppressed XOD activity, and improved renal damage. Analysis by 16S rRNA sequencing revealed that both diosmetin and quercetin supplementation increased the abundance of beneficial bacteria, such as *Lactobacillus johnsonii*, and reduced the abundance of harmful bacteria, such as *Desulfovibrio fairfieldensis*. Notably, diosmetin shows lower potential hepatotoxicity than quercetin, as evidenced by the restoration of alanine aminotransferase (ALT) and aspartate aminotransferase (AST) levels in HUA-induced liver injury and a higher binding docking score with the p38MAPK protein. These findings provide a robust scientific basis for developing natural therapeutics with enhanced efficacy and safety.

Keywords: Hyperuricemia; Xanthine oxidase; Diosmetin; Quercetin; Molecular docking; 16S rRNA.

1. Introduction

Hyperuricemia (HUA), a clinical syndrome induced by purine metabolism disorders, has rapidly increased in incidence worldwide in parallel with modern lifestyle changes [1]. The global prevalence rate has been documented to range from 2.6% to 36% across different populations, with a notably pronounced trend of younger-onset cases [2]. Sustained high serum uric acid levels cause complications such as gouty arthritis and uric acid nephrolithiasis [3]. Hyperuricemia also acts as an independent risk factor for metabolic syndrome, cardiovascular diseases, and chronic kidney disease, forming a vicious cycle of multisystem damage, and it has emerged as a major global public health challenge requiring urgent resolution [4]. Xanthine oxidase (XOD) inhibitors (allopurinol and febuxostat), as current first-line drugs, effectively suppress uric acid production;

[#]These authors have contributed equally to this work.
***Corresponding author**
512649113@qq.com (W. L. Sun). yanfei_z@163.com (Y.F. Zheng).

Received 14 November 2025
Received in revised from 29 December 2025
Accepted 5 February 2026

however, they have significant persistent limitations [5]. Clinical studies have demonstrated that XOD inhibitors may induce severe hypersensitivity reactions, hepatorenal dysfunction, and increased cardiovascular risk [6]. Notably, allopurinol hypersensitivity syndrome has a mortality rate of 20-25% [7], while cardiovascular safety concerns with febuxostat have prompted an FDA black box warning [8]. These therapeutic dilemmas underscore the critical need for developing novel agents with enhanced efficacy and improved safety profiles.

Dietary flavonoids have garnered substantial interest in medicine and nutritional science owing to a favorable safety profile and multi-target pharmacological potential [9]. These flavonoid compounds are widespread in common foods and medicinal plants, such as onions (*Allium cepa*, quercetin) [10], citrus fruits (*Citrus* species, diosmetin) [11], celery (*Apium graveolens*, luteolin) [12], and *Scutellaria baicalensis* (baicalein) [13], making them readily accessible for dietary intervention. Notably, many of these flavonoid-rich sources have been traditionally employed across cultures to alleviate symptoms associated with "dampness", swelling, and joint discomfort, which closely mirror the clinical manifestations of hyperuricemia and gout [14]. For instance, citrus and celery have historically been consumed for their diuretic and anti-inflammatory properties [15], while onions are often incorporated into diets to support cardiovascular and metabolic health [16]. This historical use provides empirical evidence supporting the hypothesis that dietary flavonoids are beneficial for hyperuricemia management. Beyond their traditional medicinal value, modern epidemiological and clinical studies have further validated the broad health benefits and excellent safety profile of dietary flavonoids, which are particularly critical for chronic disease management [17]. Epidemiological evidence indicates that a daily intake of 300–500 mg of flavonoids significantly reduces the risk of cardiovascular disease, type 2 diabetes, and hypertension [18]. Compared with synthetic pharmaceuticals, dietary flavonoids demonstrate exceptionally low hepato-renal toxicity and hypersensitivity incidence, with clinical data revealing an adverse reaction rate of less than 0.5%. These attributes position dietary flavonoids as ideal candidates for the long-term management of chronic metabolic disorders, such as HUA. However, the structure-activity relationship (SAR) between dietary flavonoids and XOD remains inadequately understood, and the underlying mechanisms of their interaction are still not fully characterized. Recently, emerging computational approaches, including SWISS-MODEL-based protein structure prediction and molecular docking simulations, have been employed as innovative strategies to decipher flavonoid-XOD interactions. These approaches provide critical insights into how specific structural features (hydroxylation patterns and methoxylation sites) modulate XOD inhibitory activity.

Studies have demonstrated that the gut microbiota is intricately linked to host physiological homeostasis. However, XOD inhibitors, such as allopurinol and febuxostat, have consistently exhibited detrimental effects on the gut microbiota [19]. For example, allopurinol treatment increased the abundance of pathogenic bacteria such as *Klebsiella*, while the recovery effect of probiotics such as *Lactobacillus* was limited [20]. This imbalance may aggravate the host's metabolic disorders by activating intestinal inflammatory pathways [21]. Another study on febuxostat revealed that the drug reduced the abundance of urease-related bacteria such as *Eubacterium*, *Parabacteroides*, and *Ruminococcus* by inhibiting urease activity in the intestinal flora [22]. This

change may interfere with the enterohepatic circulation of urea-ammonia, leading to an increase in blood ammonia levels, which in turn increases the burden on the kidneys [23]. Moreover, febuxostat also significantly reduced the abundance of short-chain fatty acid (SCFA)-producing bacteria, such as *Lactobacillus* and *Bifidobacterium* [24]. These bacteria are associated with impaired intestinal barrier function and an enhanced inflammatory response. This disruption of drug-microbiota interactions may partially explain the acquired drug resistance and aggravated hepatorenal toxicity [25]. Recently, emerging evidence has suggested that dietary flavonoids exert beneficial effects on the gut microbial composition by selectively promoting the growth of beneficial bacteria (*Bifidobacterium* and *Lactobacillus*) while suppressing pathogenic species (*Desulfovibrio*) [26, 27]. Therefore, dietary flavonoid-derived XOD inhibitors may be a way to address the limitations of allopurinol and febuxostat in the intestinal flora.

This study first established the SAR of dietary flavonoids against XOD through systematic *in vitro* activity screening. Subsequently, integrative computational approaches employing SWISS-MODEL-based docking and enzyme kinetic analyses mechanistically were applied to decipher the molecular determinants governing flavonoid-XOD interactions. Concurrently, the anti-hyperuricemic and XOD inhibitory activities of dietary flavonoids *in vivo* were evaluated in a hyperuricemic mouse model. Furthermore, we comprehensively evaluated the safety profile of dietary flavonoids by assessing their regulatory effects on the gut microbiota via 16S rRNA sequencing and predicting their potential hepatotoxicity through molecular docking. These findings not only overcome the trade-off between efficacy and safety that limits current urate-lowering therapies, but also provide a mechanistic framework for developing flavonoid nutraceuticals as adjuvant strategies against hyperuricemia.

2. Methods

2.1 Materials and Reagents

Apigenin (HPLC purity ≥ 98%), diosmetin (HPLC purity ≥ 99%), naringenin (HPLC purity ≥ 98%), kaempferol (HPLC purity ≥ 98%), hyperoside (HPLC purity ≥ 97%), rutin (HPLC purity ≥ 98%), baicalein (HPLC purity ≥ 98%), 5,7-dimethoxyflavone (HPLC purity ≥ 98%), and galangin (HPLC purity ≥ 98%) were purchased from Macklin Biochemical Technology Co., Ltd., Shanghai, China. Chrysin (HPLC purity ≥ 98%) and luteolin (HPLC purity ≥ 98%) were purchased from Aladdin Biochemical Technology Co., Ltd., Shanghai, China. Tricin (HPLC purity ≥ 96%), quercetin (HPLC purity ≥ 98%), flavone (HPLC purity ≥ 98%), 7-hydroxyflavone (HPLC purity ≥ 98%), 5-methoxyflavone (HPLC purity ≥ 98%), 5,6,7-trimethoxyflavone (HPLC ≥ purity 97%), oroxin A (HPLC purity ≥ 98%), oroxin B (HPLC purity ≥ 98%), myricetin (HPLC purity ≥ 98%) and allopurinol (HPLC purity ≥ 98%) were purchased from Yuanye Bio-Technology Co., Ltd., Shanghai, China. Xanthine (HPLC purity ≥ 99.5%), xanthine oxidase (XOD, 50 U/mg) and sodium hydroxide (NaOH, > 99%) were purchased from Macklin Biochemical Technology Co., Ltd., Shanghai, China. Dimethylsulfoxide (DMSO, > 99%) was purchased from Solarbio Co. Ltd., Beijing, China. Phosphate-buffered saline (PBS, 1×, pH 7.4) and hydrochloric acid (HCL, > 99%) were purchased from Biosharp Biochemical Technology Co., Ltd., Shanghai, China.

2.2 Evaluation of XOD Activity

A 50-μL aliquot of each sample was mixed with 50 μL of 0.2 U/mL XOD protein solution and incubated for 30 min at 37℃. Subsequently, 100 μL of 150 μM xanthine solution was added to initiate the enzymatic reaction, followed by a 15 min incubation. The absorbance of this test group was measured at 290 nm using a Varioskan Flash microplate reader (Thermo Fisher Scientific (China) Co., Ltd., Shanghai, China) and recorded as A_1. Additionally, a sample blank group (without XOD protein, absorbance recorded as A_i), a control experimental group (DMSO instead of sample, absorbance recorded as A_0) and a control blank group (without sample and XOD protein, absorbance recorded as A_2) were included. The total reaction volume was maintained at 200 μL. After initiation of the reaction, absorbance readings were acquired every 20 s until stabilization. All the assays were performed in triplicate [28]. The XOD inhibition rate (%) was calculated using the following formula:

$$\text{XOD inhibition rate}\ (\%)=(1-\frac{A_1-A_i}{A_0-A_2})\times 100 \quad (1)$$

2.3 Determination of XOD Inhibition Kinetics

The Michaelis-Menten and Lineweaver-Burk models were used to determine the kinetic mode of inhibition of diosmetin or quercetin against XOD. The reaction activities of different concentrations of dietary flavonoids (0, 12.5, 25, and 50 μmol/L) at varying concentrations of XOD protein (0.10, 0.20, 0.30 and 0.40 U/mL) were determined when the concentration of substrate was kept at 100 μmol/L, and the reaction rate change curve illustrated the reversibility of the inhibition. The type of XOD inhibited by the inhibitors (diosmetin or quercetin) was investigated using the Lineweaver-Burk equation (Eq. (2), double reciprocal form). The enzymatic reaction velocity (v, ΔA/min) was determined for different concentrations of diosmetin or quercetin (0, 12.5, 25 and 50 μmol/L) with varying concentrations of xanthine (60, 120, 240 and 480 μmol/L) at a constant concentration of XOD (0.25 U/mL) [29]. For mixed inhibition, the Lineweaver-Burk equation can be expressed as follows:

$$\frac{1}{v}=\frac{K_m}{V_{max}}\left(1+\frac{[I]}{K_i}\right)\frac{1}{[S]}+\frac{1}{V_{max}}\left(1+\frac{[I]}{\alpha K_i}\right) \quad (2)$$

The secondary plots were determined using the following formula:

$$\text{Slope}=\frac{K_m}{V_{max}}+\frac{K_m[I]}{V_{max}K_i} \quad (3)$$

$$\text{Y-Intercept}=\frac{1}{V_{max}^{app}}=\frac{1}{V_{max}}+\frac{1}{\alpha K_i V_{max}}[I] \quad (4)$$

where v is the reaction rate of the enzyme. V_{max} and V_{max}^{app} are the maximum and apparent maximum enzymatic reaction rates, respectively. K_i and K_m are the inhibition constant and Michaelis-Menten constant, respectively. α represents the apparent constant. [S] and [I] represent the concentrations of xanthine and diosmetin or quercetin, respectively.

2.4 Molecular Docking

The X-ray crystal structure of XOD complexed with quercetin (PDB ID 3NVY; resolution 2.00 Å) was obtained from the Protein Databank (PDB, https://www.rcsb.org/) and uploaded into the Chimera 1.14 workspace. Hydrogens and AMBER charges were added, followed by energy minimization using 200 steepest descent steps and 10 conjugate gradient steps. All nonstandard residues (dioxothiomolybdenum (iv) ions, molybdopterin and water molecules) were removed. The 3D structures of diosmetin, quercetin, allopurinol, and xanthine were downloaded from PubChem (https://pubchem.ncbi.nlm.nih.gov/). The downloaded structures were uploaded into the Open Babel plugin workspace of PyRx docking software for energy minimization and then converted into Schrödinger Maestro-compliant (or pdbqt) ligands. Subsequently, hydrogenation and charge calculations were performed using Schrödinger Maestro 16.0, and the results were saved in PDBQT format for backup. Using the same center (x = 45.41, y = 22.33, z = 20.56), two different grid boxes were generated: a (20 Å × 20 Å × 20 Å) cube for the active site and a (36 Å × 36 Å × 36 Å) cube for the allosteric pocket, both with 0.375 Å spacing. The number of runs was set at 100, and the other parameters remained unchanged. The hydrogen bonds between dietary flavonoids (diosmetin or quercetin) and XOD were visualized using the PyMOL molecular graphics system [30].

The binding affinity of diosmetin or quercetin for the liver injury core target was identified via molecular docking. p38α, the major p38 MAPK isoform, plays a crucial role in liver injury [31-33]. The structure of p38 (PDB ID 5OMH; resolution 2.50 Å) was downloaded from the PDB database. The molecular docking procedure was performed as previously described [34], with a docking score lower than 8 points adopted as the screening criterion for identifying potential hepatotoxic compounds[34].

2.5 Protein Structure Prediction via SWISS-MODEL

The three-dimensional structure of the mutated target protein was predicted using the automated modeling pipeline of SWISS-MODEL. The target amino acid sequence was submitted to the SWISS-MODEL server (https://swissmodel.expasy.org/), which was used to perform a template search against the SWISS-MODEL template library using BLAST and HHblits to identify suitable structural homologs. The highest-quality template was selected on the basis of sequence identity (≥ 70 %) and resolution (≤ 2.5 Å). Model construction employed default global optimization parameters (global model quality estimation, GMQE ≥ 0.85) to ensure structural reliability.

2.6 Animal Experimental Protocol

Six-week-old male KM mice were purchased from the Shandong Experimental Animal Center (Permission no. SCXK 2020-0006, Jinan, China). All the mice were maintained in a controlled environment with an optimal temperature and humidity and under a standardized 12-hour light/dark cycle. Our animal experiments conformed to international ethical guidelines and were approved by the Institutional Animal Care and Use Committee of Shandong University of Technology (YLX202403012).

HUA model mice were intraperitoneally injected with potassium oxonate (PO, 250 mg/kg·d) and provided access to water containing 5% fructose ad libitum. The mice were randomly divided into groups according to body weight. After one week of acclimation to the experimental environment, the groups of

experiments were organized as follows: 56 specific pathogen-free (SPF) KM mice were randomly divided into seven groups: the NC group (n = 8, standard diet), the HUA group (n = 8, daily gavage of normal saline), the DML group (n = 8, daily gavage of 10 mg/kg diosmetin), the DMH group (n = 8, daily gavage of 50 mg/kg diosmetin), the QRL group (n = 8, daily gavage of 10 mg/kg quercetin), the QRH group (n = 8, daily gavage of 50 mg/kg quercetin) and the AP group (n = 8, daily gavage of 5 mg/kg allopurinol). During the final week of the study, urine and faeces were collected from mice housed in metabolic cages. At the end of the experiment, blood was withdrawn from the retro-orbital venous plexus under isoflurane anaesthesia, and plasma was separated by centrifugation (3000 × g, 10 min, 4℃) and stored at –80℃ until analysis. Immediately thereafter, animals were euthanised by controlled CO_2 asphyxiation, and death was confirmed by cervical dislocation.Tissues were rapidly excised, snap-frozen in liquid nitrogen, and stored at –80℃, or immersed in 4 % paraformaldehyde for histological examination.

2.7 Biochemical Indicators

Commercial assay kits for creatinine (cat. C011-2-1), blood urea nitrogen (cat. C013-2-1), xanthine oxidase (cat. A002-1-1), alanine aminotransferase (cat. C009-2-1) and aspartate aminotransferase (cat. C010-2-1) were obtained from Nanjing Jiancheng Bioengineering Institute Co., Ltd. (Nanjing, China). The uric acid assay kit (cat. BC1360-50T/24S) was purchased from Beijing Solarbio Science & Technology Co., Ltd. (Beijing, China). The BCA protein quantification kit (cat. CW0014S) was supplied by Cowin Bioscience Inc. (Jiangsu, China).

2.8 Histological Examination

The kidneys were immersed in 4% paraformaldehyde for fixation. In accordance with the manufacturer's instructions, the kidney samples were embedded in paraffin and sliced into 3 μm sections, which were subsequently stained with an H&E stain kit (Solarbio). All the sections were examined under a microscope, and pathological analyses were performed.

2.9 16S rRNA sequencing Analysis

Gut microbiota genomic DNA was extracted from feces using the EZNA® soil DNA Kit. The DNA samples were examined by 1% agarose gel electrophoresis and NanoDrop2000 analysis to assess DNA quality. PCR amplification focusing on the V3-V4 region of the 16S rRNA gene was subsequently performed using FastPfu polymerase and dedicated primer sets. The PCR cycling conditions were as follows: initial denaturation at 95℃ for 3 minutes; 27 cycles of denaturation at 95℃ for 30 seconds, annealing at 55℃ for 30 seconds, and extension at 72℃ for 45 seconds; and a final extension at 72℃ for 10 minutes. The upstream primer used was 338F (5'-ACTCCTACGGGAGGCAGCAG-3'), whereas the downstream primer used was 806R (5'-GGACTACHVGGGTWTCTAAT-3'). PCR of each sample was replicated three times to ensure reproducibility. The PCR products generated from each identical sample were pooled and purified using a commercially available purification kit. The purified PCR products were further cleaned using an AxyPrep DNA gel extraction kit and visualized by 2% agarose gel electrophoresis. The precise concentration and

quantity of the PCR products were subsequently determined using a Quantus™ Fluorometer (Promega, USA). The Illumina MiSeq PE300/NovaSeq PE250 platform was utilized for sequencing to generate high-quality sequencing data. The sequences were subjected to quality filtering to ensure reliability and accuracy.

After the samples were distinguished, operational taxonomic unit (OTU) cluster analysis and species taxonomy analysis were performed. On the basis of the OTU cluster analysis results, the sequencing depth was detected. On the basis of taxonomic information, a statistical analysis of community structure was performed at various taxonomic levels. Bioinformatics analysis of the gut microbiome was performed with a bioinformatics platform: Majorbio Cloud (https://cloud.majorbio.com). The Sobs index and Shannon index were computed via Mothur v1.30.1, leveraging the OTU data. The Kruskal-Wallis test was used for statistical assessment of differences in alpha diversity among the NC, HUA, DML, DMH, QRL and QRH groups. The beta diversity was calculated on the basis of the Bray-Curtis distance. The relative abundances of phyla and genera were calculated according to the dominant bacteria. Linear discriminant analysis effect size (LEfSe) analysis was employed to identify the characteristic bacterial composition in the NC, HUA, DML, DMH, QRL and QRH groups. The sequence data were submitted to the NCBI Sequence Read Archive under accession number PRJNA1294550.

2.10 Statistical analyses

All the data are shown as the means ± standard errors of the mean (SEMs), and the data were processed using GraphPad Prism 9.5. Differences among experimental groups were analyzed using the unpaired t test or one-way ANOVA with Tukey's post hoc test. A difference was deemed statistically significant when $P < 0.05$. In the figures, distinct alphabetical markers indicate significant differences between the two groups. For half-maximal inhibitory concentration (IC_{50}) values, data are presented as the means ± standard deviations (SDs)

3. Results

3.1 Inhibitory effect of dietary flavonoids on XOD

Using xanthine as the substrate, we evaluated the XOD inhibitory rates of 20 dietary flavonoids, whose ball-and-stick structures are depicted in Fig. 1. Table 1 summarizes the IC_{50} values of these dietary flavonoids at 75 μmol/L xanthine. A systematic summary of the SAR between the structural modifications of these flavonoids and their XOD inhibitory potencies is visualized in Fig. 2. The parent flavone scaffold (labeled with A/B/C rings) serves as the reference in this figure. Structural modifications (e.g., hydroxylation, methoxylation, glycosylation) at specific positions of the A/B/C rings are directly correlated with the corresponding IC_{50} values of individual flavonoids. For the A-ring substitutions of flavonoids, a positive correlation was observed between the number of hydroxyl groups and XOD inhibitory activity, as reflected by the IC_{50} values: flavone > 7-hydroxyflavone > chrysin > baicalein (Fig. 3A). Moreover, a positive correlation was also observed between the number of methoxyl groups and XOD inhibitory activity, as reflected by the IC_{50} values: flavone > 5-methoxyflavone > 5,7-dimethoxyflavone > 5,6,7-trimethoxyflavone (Fig. 3B). In contrast, increased glycosylation of the A-ring in flavonoids was negatively correlated with XOD

inhibitory activity, as demonstrated by the following IC_{50} values: oroxin B > oroxin A > baicalein (Fig. 3C). Interestingly, increased hydroxyl substitutions on the B-ring of flavonoids did not increase XOD inhibitory activity, as evidenced by the IC_{50} values, which were as follows: galangin > kaempferol > myricetin > quercetin (Fig. 3D). Moreover, increased methoxyl substitutions on the B-ring of flavonoids did not increase XOD inhibitory activity, as evidenced by the IC_{50} values, which were as follows: chrysin > tricin > luteolin> diosmetin (Fig. 3E). For the C-ring substitutions of flavonoids, a greater number of hydroxyl groups were positively correlated with XOD inhibition, with IC_{50} values in the order apigenin > kaempferol (Fig. 3F). Notably, the presence of a C2=C3 double bond in the C-ring significantly increased XOD inhibitory activity, as evidenced by the following IC_{50} values: naringenin > apigenin (Fig. 3G). In contrast, increased glycosylation of the C-ring in flavonoids was negatively correlated with XOD inhibitory activity, as demonstrated by the following IC_{50} values: rutin > hyperoside > quercetin (Fig. 3H). The above observations suggested that diosmetin (IC_{50} = 2.76±0.03 μmol/L) and quercetin (IC_{50} = 2.41±0.68 μmol/L) exhibited the highest inhibitory potencies among the dietary flavonoids. The SAR study emphasized that the structural characteristics of flavonoids critically influence their ability to mediate XOD inhibition.

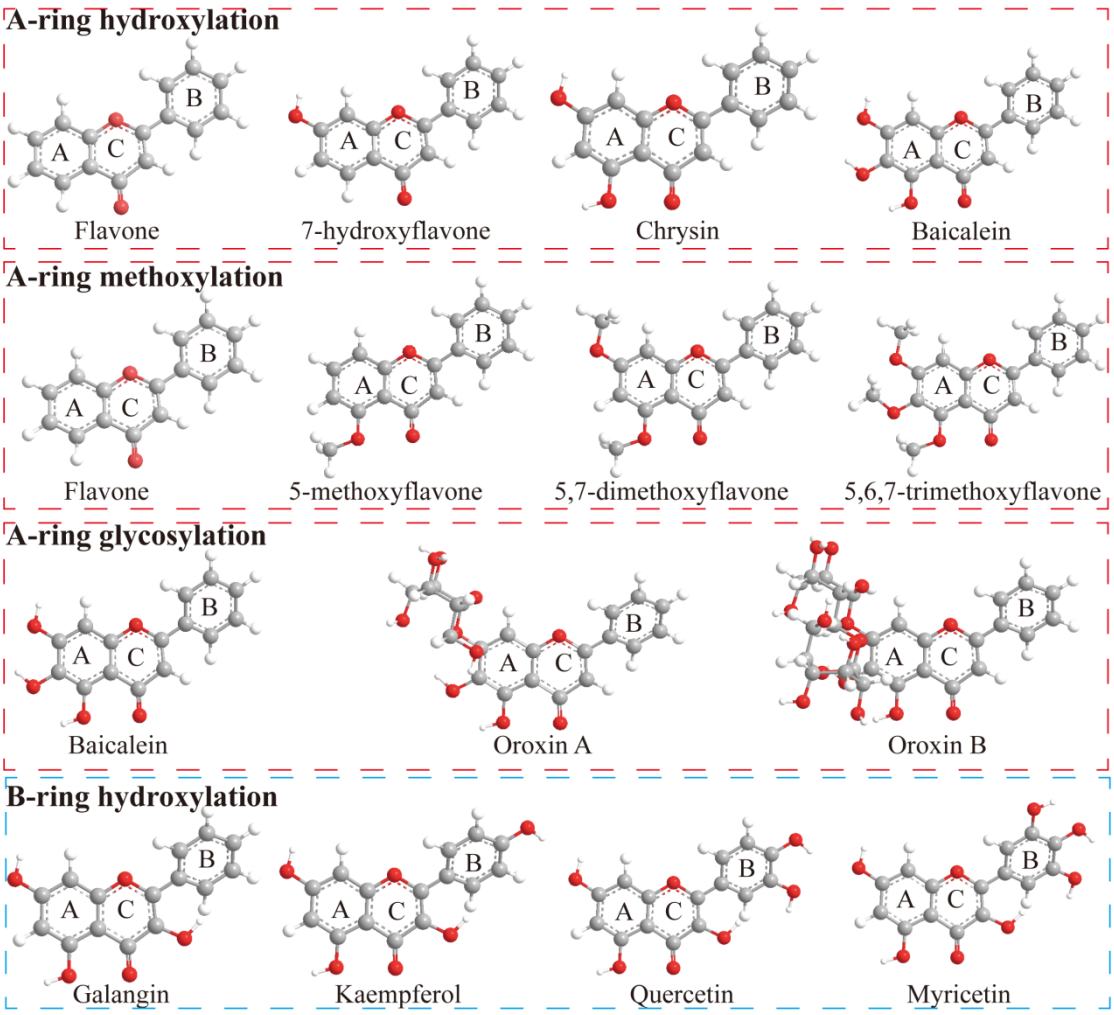

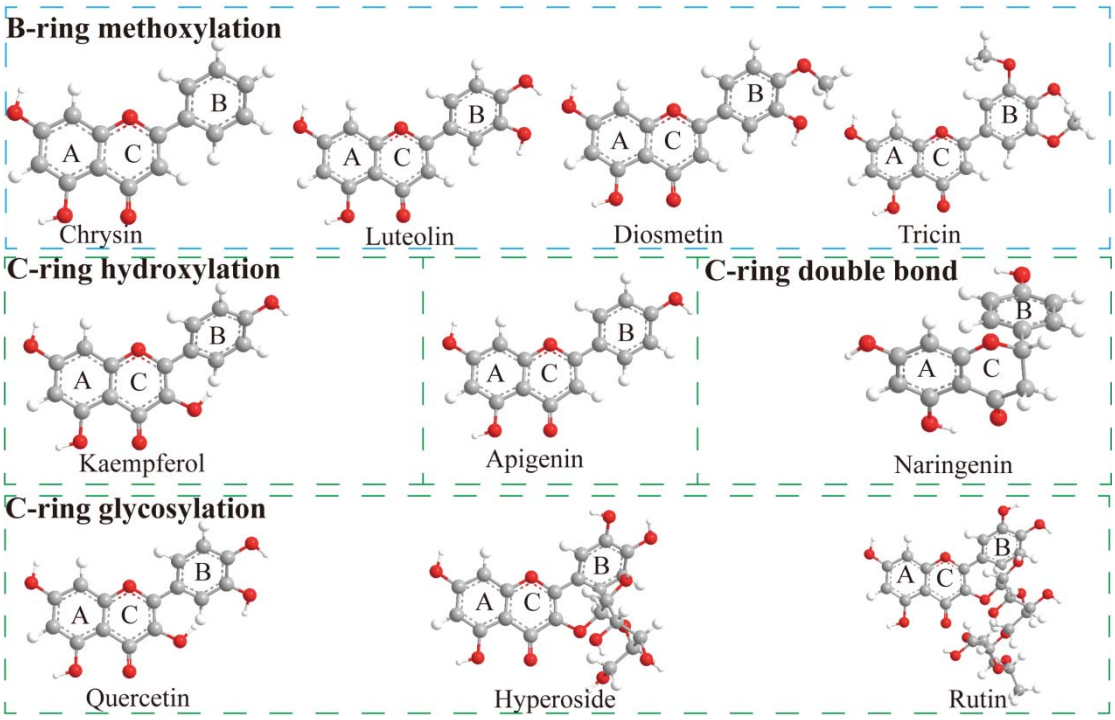

Fig. 1. Ball-and-stick models of 20 dietary flavonoid compounds categorized by structural modifications. The ball-and-stick models illustrate the chemical structures of 20 flavonoids, grouped by modification types (A-ring/B-ring/C-ring hydroxylation, methoxylation, glycosylation, and C-ring double bond variation).

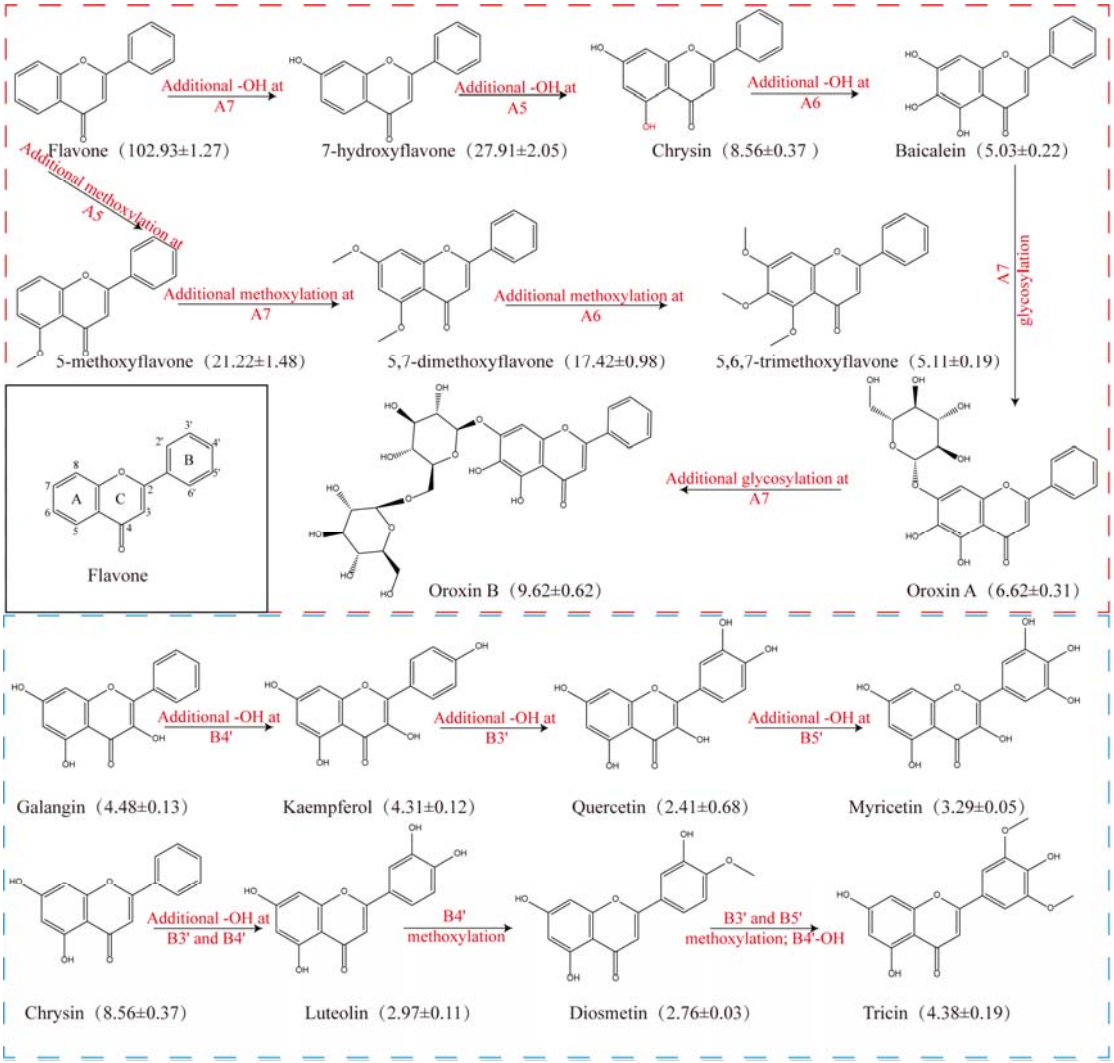

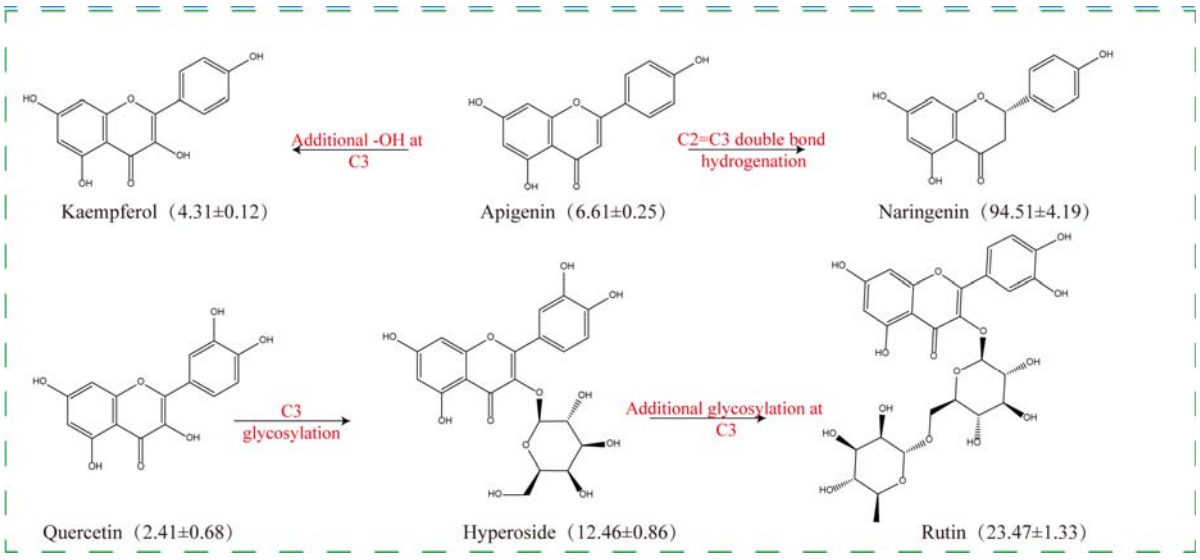

Fig. 2 Structure-activity relationships of 20 dietary flavonoids based on their XOD inhibitory potencies (IC_{50} values, μmol/L, mean ± SD).

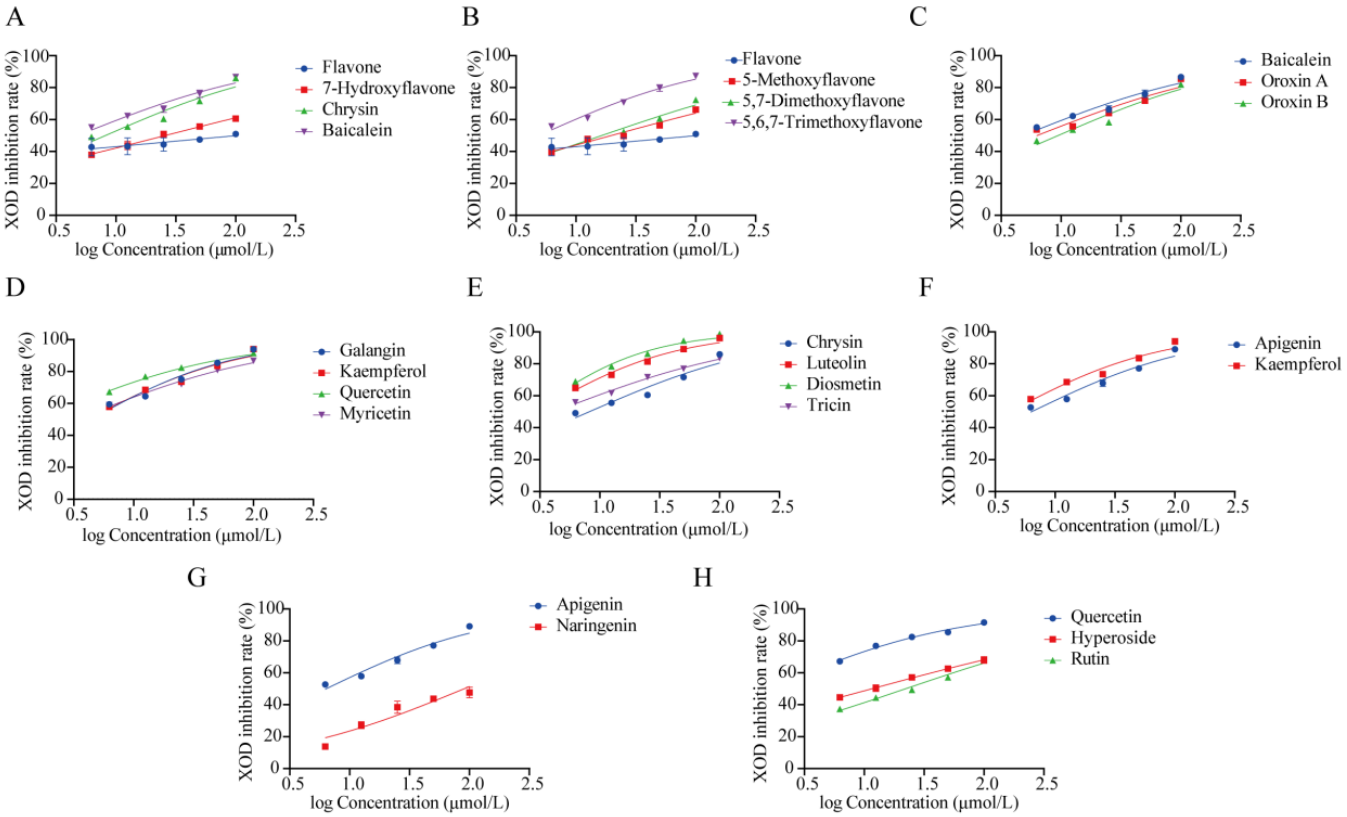

Fig. 3 Dose-response curves of XOD inhibition rate for 20 flavonoid compounds. (A) Flavone, 7-hydroxyflavone, chrysin, and baicalein. (B) Flavone, 5-methoxyflavone, 5,7-dimethoxyflavone, and 5,6,7-trimethoxyflavone. (C) Oroxin A, oroxin B, and baicalein. (D) Quercetin, galangin, kaempferol, and myricetin. (E) Chrysin, luteolin, diosmetin, and tricin. (F) Apigenin and kaempferol. (G) Naringenin and apigenin. (H) Quercetin, hyperoside, and rutin. Dose–response curves of XOD inhibition rate versus concentration for 20 flavonoid compounds.

Table 1. Sources, traditional uses, IC_{50} values, and molecular docking scores of 20 flavonoid derivatives.

Compounds	Source	Traditional use	IC_{50} (μmol/L)	Docking Score	Refs
Quercetin	*Malus domestica*, *Allium cepa*, *Camellia sinensis*, berry fruits	Clears heat-toxin, cools blood, relieves swelling; used for sore throat, damp-heat jaundice.	2.41±0.68	–6.769	[66, 67]
Diosmetin	*Rosmarinus officinalis*, *Citrus sinensis*, *Galium verum*, *Rosa agrestis*	Regulates qi, relieves stagnation, clears damp-heat; used for abdominal distension, damp-heat diarrhea.	2.76±0.03	–6.065	[68, 69]
Luteolin	A*pium graveolens*, *Brassica oleracea*, *Citrus navel*, *Taraxacum* spp., *Mentha* spp., *Rosmarinus officinalis*	Clears heat, disperses wind-heat; used for wind-heat cold, sore throat, boils.	2.97±0.11	–6.731	[12, 70, 71]
Myricetin	Berry fruits, *Citrus* spp., *Vitis vinifera*, herbal teas, wine	Astringes diarrhea, promotes fluid production; used for diarrhea, thirst.	3.29±0.05	–6.576	[72-75]
Kaempferol	*Spinacia oleracea*, *Brassica oleracea*, *Allium fistulosum*, *Zingiber officinale*, *Camellia sinensis*	Antioxidant, clears heat-toxin; food sources widely used for common cold, eye irritation.	4.31±0.12	–6.250	[76-79]
Tricin	*Oryza sativa*, *Hordeum vulgare*, *Avena sativa*, *Triticum aestivum*	Supports digestion; bran of rice/wheat traditionally used for food stagnation, mild diarrhea.	4.38±0.19	–6.157	[80-83]
Galangin	*Alpinia officinarum*, honey	Source plant (Alpinia officinarum) warms middle-jiao and stops vomiting.	4.48±0.13	–5.772	[84, 85]
Baicalein	*Scutellaria baicalensis* (trace in *Thymus vulgaris*, *Apium graveolens*)	Drains damp-heat & fire-toxin; used for damp-warm fever, jaundice, dysuria.	5.03±0.22	–4.853	[86]
5,6,7-Trimethoxyflavone	*Callicarpa japonica*, *Zeyhera tuberculosa*, *Friesodielsia velutina*	Externally used for eczema and wound bleeding; no recorded internal traditional use.	5.11±0.19	–6.485	[87, 88]
Apigenin	*Matricaria chamomilla*, *Petroselinum crispum*, *Fortunella spp.*, *Apium graveolens*	Calms liver, clears heat, dispels wind, promotes diuresis; used for headache, dizziness, dysuria.	6.61±0.25	–6.526	[89-92]
Oroxin A	*Oroxylum indicum*	Clear the lungs, drain heat-toxin and resolve phlegm; used for sore throat and lung-heat cough.	6.62±0.31	–5.357	[93]
Chrysin	Honey, propolis, *Passiflora edulis*	Clears heat-toxin, resolves phlegm; used for sore throat, lung heat cough.	8.56±0.37	–5.782	[94, 95]
Oroxin B	*Oroxylum indicum*	Clear the lungs, drain heat-toxin and resolve phlegm; used for sore throat and lung-heat cough.	9.62±0.62	–6.046	[96]
Hyperoside	*Aronia melanocarpa*, *Juglans regia*□*Rumex acetosa*, *Crataegus pinnatifida*, *Vitis vinifera*, *Vaccinium macrocarpon*	Soothes liver, regulates qi, promotes blood circulation; used for chest distension, blood stasis.	12.46±0.86	–5.708	[97-100]
5,7-Dimethoxyflavone	*Kaempferia parviflora*□*Boesenbergia rotunda*□*Citrus* spp	Regulates qi, invigorates spleen, dries dampness; used for abdominal distension, poor appetite.	17.42±0.98	–5.646	[101, 102]
5-Methoxyflavone	*Mentha* spp.□*Kaempferia parviflora*□*Hibiscus rosa-sinensis*□*Citrus* spp.	Trace constituent with no standalone ethnomedical indication; source plants used for dyspepsia (mint), hypertension (roselle).	21.22±1.48	–5.192	[101]
Rutin	*Fagopyrum esculentum*□*Robinia pseudoacacia*□*Ginkgo biloba*□*Citrus* peel	Cools blood, stops bleeding, clears liver fire; used for hemorrhoids, eye redness.	23.47±1.33	–4.272	[103-106]
7-Hydroxyflavone	*Scutellaria baicalensis*□*Matricaria recutita*□*Thymus vulgaris*	Purges fire, dispels wind, detoxifies; used for headache, sore throat.	27.91±2.05	–6.095	[107]
Naringenin	*Citrus paradisi*□*Citrus sinensis*, *Citrus maxima*, *Citrus limon*□*Citrus paradisi*□*Citrus aurantium*	Regulates qi, relieves stagnation, resolves phlegm; used for abdominal distension, cough with phlegm.	94.51±4.19	–4.222	[108-111]
Flavone	*Myrtaceae* pollen	Anti-inflammatory and detumescent.	102.93±1.27	–3.06	[112]

3.2 Kinetics of the inhibitory effects of diosmetin or quercetin on XOD

Kinetic analyses revealed reversible inhibition by diosmetin, as evidenced by the linear plots intersecting at the origin with inhibitor-dependent slope reductions (Fig. 4A). Lineweaver-Burk analysis revealed mixed inhibition by diosmetin, with intersecting regression lines in the second quadrant, increased slopes and y-intercepts, and a dose-dependent increase in K_m (Fig. 4B). Molecular docking simulations were conducted via Schrödinger software to assess the binding interactions of diosmetin, xanthine, and allopurinol at the active site of XOD. The docking scores (kcal/mol), ranked in ascending order (Table 2), were as follows: diosmetin (–6.065) < allopurinol (–5.099) < xanthine (–4.937). For the allosteric site of XOD, the docking scores (ascending order, Table 3) were: diosmetin (–6.768) < xanthine (–5.339) < allopurinol (–5.038). These results collectively classified diosmetin as a mixed-type XOD inhibitor. At the active site, molecular docking analysis showed that diosmetin formed hydrogen bonds with three amino acid residues (Asn768, Lys771, and Glu802) (Fig. 4C), with a docking score of –6.065 kcal/mol. Substitution of Asn768 with Thr yielded a docking score of –5.368 kcal/mol (Fig. 4D), whereas replacement of Lys771 with Thr resulted in –5.539 kcal/mol (Fig. S1A). The substitution of Glu802 with Thr resulted in –5.872 kcal/mol (Fig. S1B). The Asn768Thr mutation had the most pronounced effect, confirming that Asn768 was the key mediator of the competitive interaction of diosmetin. At the allosteric pocket, diosmetin bound via a salt bridge with Arg880, π–π stacking with Phe914 and Phe1009, and a hydrogen-bond network with Thr1010, Val1011, and Glu1261, with a docking score of –6.768 kcal/mol (Fig. 4E). Substitution of Arg880 with Phe yielded a docking score of –3.865 kcal/mol (Fig. S1C), whereas replacement of Phe914 with Glu resulted in –4.172 kcal/mol (Fig. S1D), and substitution of Phe1009 with Leu resulted in –3.155 kcal/mol (Fig. 4F). Substitution of Thr1010 with Ser yielded a docking score of –3.963 kcal/mol (Fig. S1E), whereas replacement of Val1011 with Leu resulted in –3.530 kcal/mol (Fig. S1F), and substitution of Glu1261 with Val resulted in a score of –4.140 kcal/mol (Fig. S1G). The Phe1009Leu mutation had the most pronounced effect, confirming that Phe1009 was the key mediator of the noncompetitive interaction of diosmetin.

Table 2. Active site molecular docking score

Compounds	Docking Score
Quercetin	–6.769
Diosmetin	–6.065
Allopurinol	–5.099
Xanthine	–4.937

Table 3. Allosteric site molecular docking score

Compounds	Docking Score
Diosmetin	–6.768
Quercetin	–5.671
Xanthine	–5.339
Allopurinol	–5.038

For quercetin, kinetic analyses revealed reversible inhibition, as evidenced by the linear plots intersecting at the origin with inhibitor-dependent slope reductions (Fig. 4G). Lineweaver-Burk analysis identified a mixed inhibition mode for quercetin, characterized by intersecting regression lines in the second quadrant, increased

slopes and y-intercepts, and a dose-dependent increase in K_m (Fig. 4H). Molecular docking simulations were conducted via Schrödinger software to assess the binding interactions of quercetin, xanthine, and allopurinol at the active site of XOD. The docking scores (kcal/mol), ranked in ascending order (Table 2), were: quercetin (–6.769) < allopurinol (–5.099) < xanthine (–4.937). For the allosteric site of XOD, the docking scores (ascending order, Table 3) were: quercetin (–5.671) < xanthine (–5.339) < allopurinol (–5.038). These results collectively classified quercetin as a mixed-type XOD inhibitor. At the active site, molecular docking analysis showed that quercetin occupied the pocket via hydrogen bonds with Lys771 and Glu802, as well as π–π stacking with Phe649 and Phe1013, with a docking score of –6.769 kcal/mol (Fig. 4I). Substitution of Phe649 with Lys yielded a docking score of –5.096 kcal/mol (Fig. S2A), whereas replacement of Lys771 with Met resulted in –4.583 kcal/mol (Fig. 4J). Substitution of Glu802 with Met yielded a docking score of –5.554 kcal/mol (Fig. S2B), and replacement of Phe1013 with Lys resulted in –5.426 kcal/mol (Fig. S2C). The Lys771Met mutation had the most pronounced effect, confirming that Lys771 was the pivotal residue mediating the competitive interaction of quercetin. At the allosteric pocket, quercetin bound via a salt bridge with Arg880, π–π stacking with Phe914 and Phe1009, and hydrogen bonds with Glu802 and Thr1010, with a docking score of –5.671 kcal/mol (Fig. 4K). Substitution of Glu802 with Ser yielded a docking score of –5.290 kcal/mol (Fig. S2D), whereas replacement of Arg880 with Phe resulted in –4.614 kcal/mol (Fig. S2E), and substitution of Phe914 with Glu yielded –4.494 kcal/mol (Fig. 4L). Additionally, replacement of Phe1009 with Glu resulted in a docking score of –4.886 kcal/mol (Fig. S2F), and substitution of Thr1010 with Ala yielded –4.626 kcal/mol (Fig. S2G). The Phe914Glu mutation caused the most significant reduction in docking score, confirming that Phe914 was the critical residue governing the noncompetitive binding of quercetin. In summary, although diosmetin and quercetin are both mixed-type XOD inhibitors, quercetin exhibited stronger binding affinity to the active site, whereas diosmetin showed a greater advantage in binding to the allosteric site. Additionally, the key amino acid residues they rely on are completely different, which may have contributed to the differences in their inhibitory efficiency and specificity.

To extend these findings, molecular docking analyses were performed for the remaining 18 dietary flavonoids, and the corresponding binding modes were visualized in Fig. S3. The docking scores of all 20 dietary flavonoids with XOD were summarized in Table 1. Moreover, a correlation analysis was performed between the docking scores and IC_{50} values of the 20 dietary flavonoids (Fig. S4). As shown in Fig. S4, a strong positive correlation was observed between the two parameters ($r = 0.8011$, $P < 0.0001$). Specifically, flavonoids with larger IC_{50} values (weaker XOD inhibitory potency) exhibited higher docking scores (weaker binding affinity to XOD), which further validates the structural basis of flavonoid-mediated XOD inhibition.

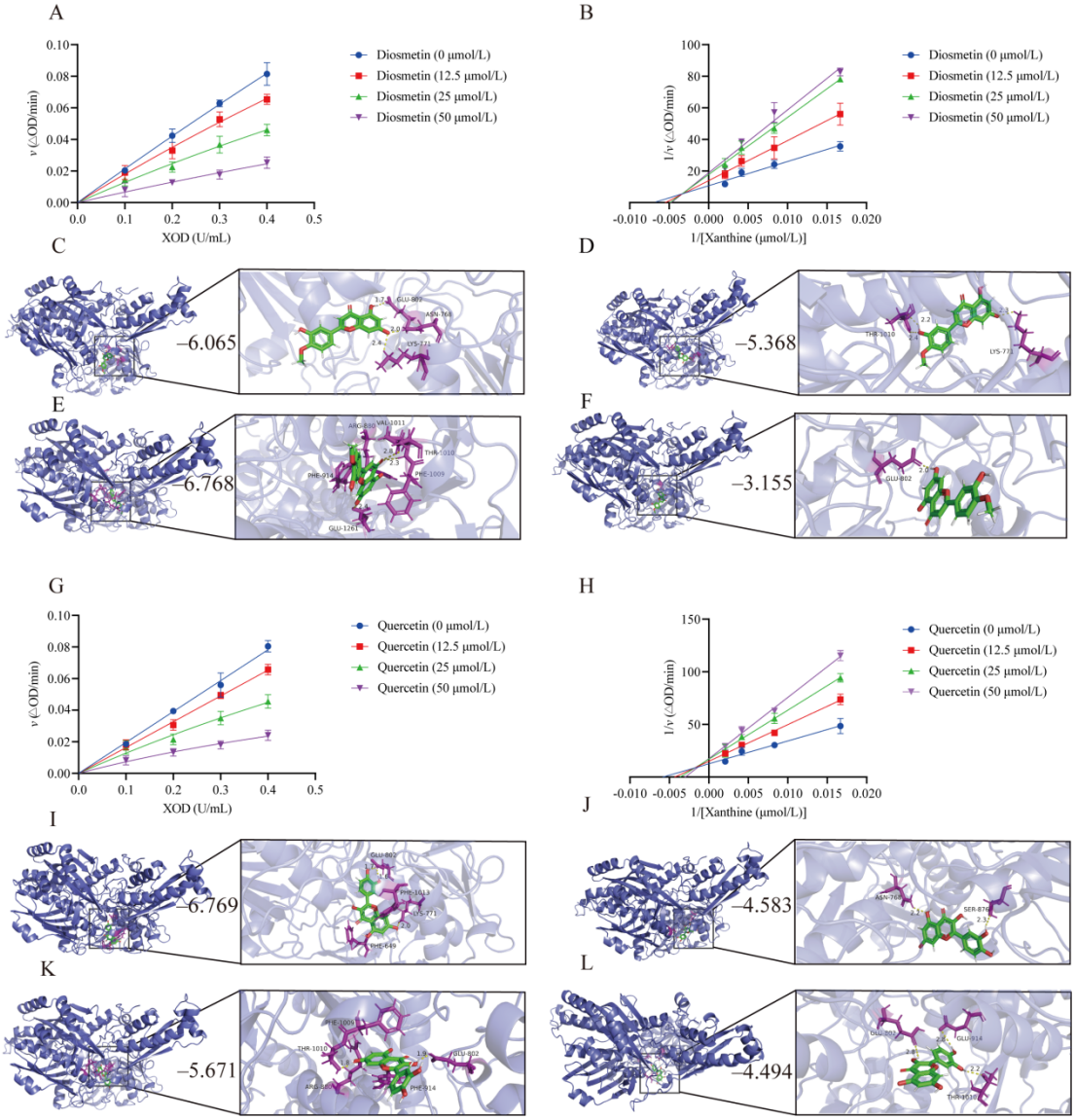

Fig. 4 Enzymatic kinetic and molecular docking analyses of diosmetin or quercetin. (A) Michaelis-Menten plots of diosmetin. (B) Lineweaver-Burk plots of diosmetin. (C) Diosmetin binding at the XOD active site. (D) Diosmetin binding to the ASN768Thr mutation at the XOD active site. (E) Diosmetin binding at the XOD allosteric site. (F) Diosmetin binding to the Phe1009Leu mutation at the XOD allosteric site. (G) Michaelis-Menten plots of quercetin. (H) Lineweaver-Burk plots of quercetin. (I) Quercetin binding at the XOD active site. (J) Quercetin binding to the Lys771Met mutation at the XOD active site. (K) Quercetin binding at the XOD allosteric site. (L) Quercetin binding to the Phe914Glu mutation at the XOD allosteric site. The atoms of diosmetin and quercetin are colored as follows: carbon, green; oxygen, red; hydrogen, white. Hydrogen bonds are indicated by yellow dashed lines.

3.3 In Vivo Validation of Diosmetin or Quercetin in Hyperuricemic Mice

The two dietary flavonoids with greater XOD inhibitory activity *in vitro*—diosmetin and quercetin—were further evaluated *in vivo* for their effects on uric acid (UA), creatinine (CRE) and blood urea nitrogen (BUN) levels in HUA mice. To assess their effects on HUA, we administered diosmetin or quercetin to HUA mice daily via oral gavage and evaluated their effects; the experimental design is depicted in Fig. 5A. Compared with those in the NC group, the HUA group presented significantly lower body weights ($P < 0.05$) (Fig. 5B), whereas both diosmetin and quercetin treatment significantly restored the body weights of HUA mice ($P < 0.05$) (Fig. 5B). Compared with those in the NC group, the serum UA levels in the HUA group were markedly elevated ($P < 0.05$) (Fig. 5C), indicating that the model was successfully established. Compared

with the HUA group, the 10 or 50 mg/kg diosmetin and the 10 or 50 mg/kg quercetin groups presented significantly lower serum UA levels ($P < 0.05$) (Fig. 5C). Notably, at the low dose (10 mg/kg), serum UA levels in the diosmetin group were significantly lower than those in the quercetin group ($P < 0.05$) (Fig. 5C). Similarly, at the high dose (50 mg/kg), serum UA levels in the diosmetin group remained significantly lower compared with the quercetin group ($P < 0.05$) (Fig. 5C). Meanwhile, compared with the HUA group, the allopurinol group also presented a significant reduction in serum UA ($P < 0.05$) (Fig. 5C). Urinary UA levels were significantly higher in HUA mice than in NC mice ($P < 0.05$) (Fig. 5D). Compared with the HUA group, the 50 mg/kg diosmetin treatment group presented increased urinary UA levels ($P < 0.05$) (Fig. 5D). In contrast, 10 mg/kg quercetin significantly decreased urinary UA levels ($P < 0.05$) (Fig. 5D), with an effect comparable to that of allopurinol (Fig. 5D). Fecal UA levels were significantly elevated in HUA mice compared with those in the NC group ($P < 0.05$) (Fig. 5E). Compared with the HUA group, the 10 or 50 mg/kg diosmetin groups presented markedly lower fecal UA levels ($P < 0.05$) (Fig. 5E), indicating a dose-dependent effect. Notably, quercetin did not reduce the fecal UA level in a dose-dependent manner (Fig. 5E). Serum CRE levels were higher in the HUA group than in the NC group ($P < 0.05$) (Fig. 5F). Compared with HUA, both 10 and 50 mg/kg diosmetin significantly decreased the serum CRE level ($P < 0.05$) (Fig. 5F). Similar results were observed with quercetin, which exerted a comparable serum CRE-lowering effect in a dose-dependent manner (Fig. 5F). Urinary CRE levels were markedly lower in HUA mice than in NC mice ($P < 0.05$) (Fig. 5G). Compared with HUA, 10 or 50 mg/kg diosmetin significantly increased urinary CRE levels ($P < 0.05$) (Fig. 5G); 50 mg/kg quercetin also increased urinary CRE levels ($P < 0.05$) (Fig. 5G) but with weaker efficacy than diosmetin ($P < 0.05$) (Fig. 5G). Serum BUN levels were significantly elevated in HUA mice relative to the NC group ($P < 0.05$) (Fig. 5H). Compared with the HUA group, the 10 or 50 mg/kg diosmetin groups presented significantly lower serum BUN levels ($P < 0.05$) (Fig. 5H). Similarly, quercetin treatment tended to decrease the serum BUN level, with both compounds exhibiting a dose-dependent effect (Fig. 5H). Urinary BUN levels were markedly lower in the HUA group compared with the NC group ($P < 0.05$) (Fig. 5I), whereas 50 mg/kg diosmetin treatment significantly increased urinary BUN levels compared with those in the HUA group ($P < 0.05$) (Fig. 5I). Quercetin treatment had a similar effect (Fig. 5I). Compared with NC mice, HUA mice presented severe renal damage, including glomerular epithelial vacuolization, thickened basement membranes, tubular dilation, and vacuolization. All the treatment groups (DML, DMH, QRL, QRH, AP) showed a mitigation of these pathological alterations, with high-dose diosmetin or quercetin resulting in near-normal renal architecture (Fig. 5J). In summary, diosmetin exhibited superior efficacy to quercetin, with more pronounced effects in lowering serum UA, increasing urinary CRE, and regulating UA excretion, especially at equivalent doses.

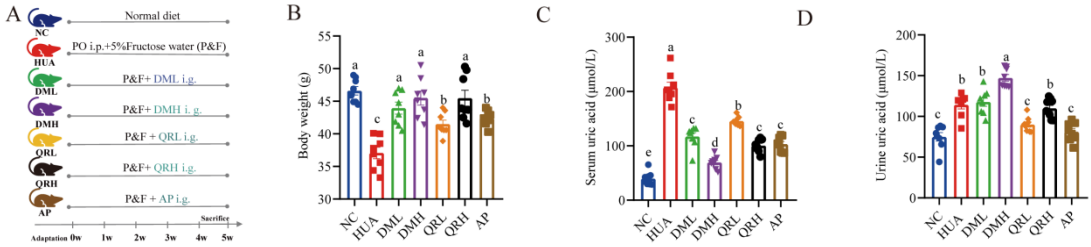

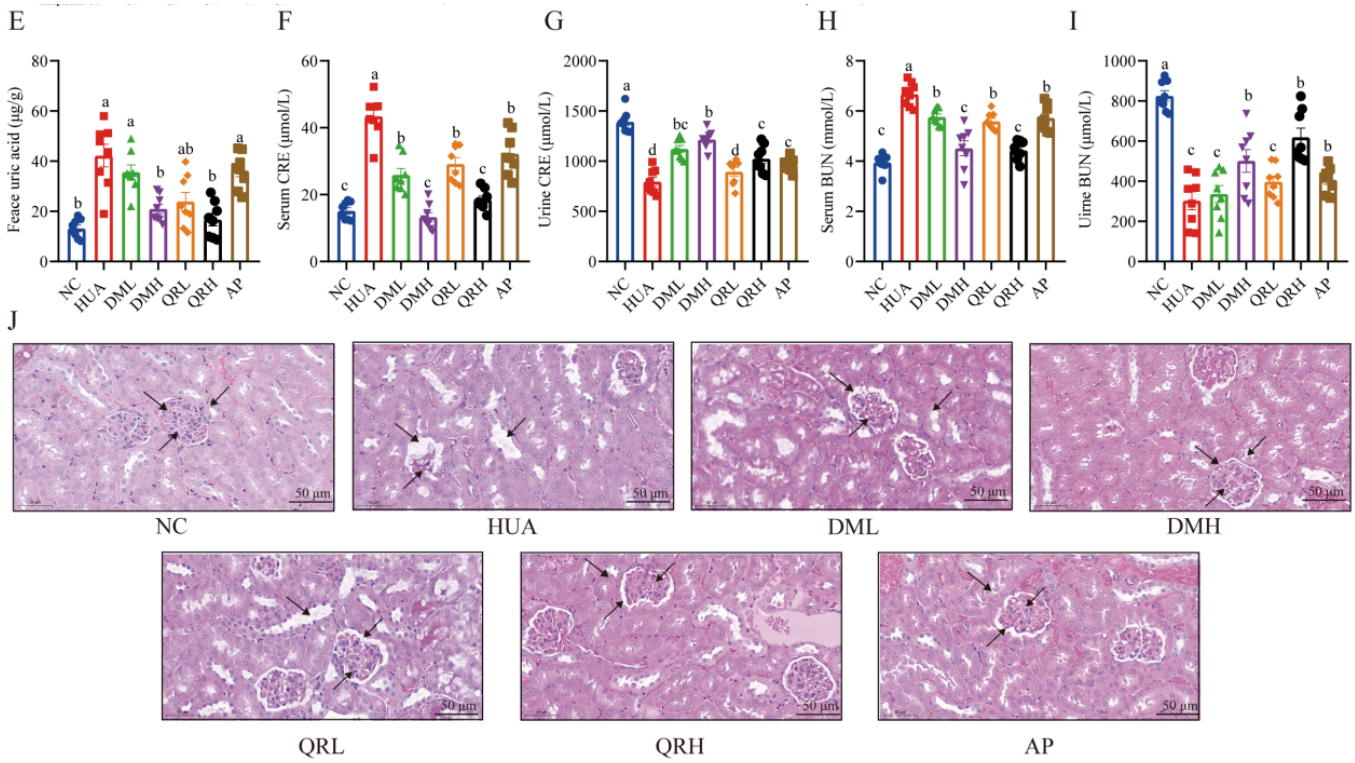

Fig. 5 Diosmetin or quercetin ameliorated PO- and fructose-induced HUA. (A) Experimental grouping and protocol for diosmetin or quercetin intervention. (B) Body weight in the last week. (C) Serum UA. (D) Urinary UA. (E) Fecal UA. (F) Serum CRE. (G) Urinary CRE. (H) Serum BUN. (I) Urinary BUN. (J) Kidney H&E staining (scale bar, 50 μm). The data are presented as the means ± SEMs of biological replicates (n = 8). Differences among experimental groups were analyzed by one-way ANOVA with Tukey's post hoc test. A difference was considered statistically significant when $P < 0.05$. Different letters indicate significant differences between the two groups. **PO**, potassium oxonate; **P&F**, intraperitoneal injection of 250 mg/kg·d PO and 5% fructose in drinking water (ad libitum); **NC**, normal control group; **HUA**, hyperuricemia group (P&F)**; DML**, low-dose diosmetin group (P&F and 10 mg/kg diosmetin); **DMH**, high-dose diosmetin group (P&F and 50 mg/kg diosmetin); **QRL**, low-dose quercetin group (P&F and 10 mg/kg quercetin); **QRH**, high-dose quercetin group (P&F and 50 mg/kg quercetin); **AP**, allopurinol group (P&F and 5 mg/kg AP); **CRE**, creatinine; **BUN**, urea nitrogen; **H&E**, hematoxylin and eosin; **XOD**, xanthine oxidase; **ANOVA**, analysis of variance.

3.4 In Vivo XOD Activity of Diosmetin or Quercetin

We subsequently investigated the effects of diosmetin or quercetin on *in vivo* XOD activity. Compared with the NC group, the HUA group presented a significant increase in serum XOD activity ($P < 0.05$) (Fig. 6A). Compared with HUA, both 10 and 50 mg/kg diosmetin significantly decreased serum XOD activity ($P < 0.05$) (Fig. 6A). However, compared with HUA, 10 mg/kg quercetin did not reduce XOD activity ($P > 0.05$) (Fig. 6B), whereas 50 mg/kg quercetin significantly decreased XOD activity ($P < 0.05$) (Fig. 6B), with effects similar to those of allopurinol (Fig. 6B). Similarly, hepatic XOD activity in HUA mice tended to increase to a level that was markedly greater than that in the NC group ($P < 0.05$) (Fig. 6C). Compared with the HUA group, both the 10 and 50 mg/kg diosmetin groups presented significantly lower hepatic XOD activity ($P < 0.05$) (Fig. 6C). In contrast, 10 mg/kg quercetin did not reduce hepatic XOD activity relative to that in the HUA group ($P > 0.05$) (Fig. 6D), whereas 50 mg/kg quercetin significantly decreased XOD activity ($P < 0.05$) (Fig. 6D), with effects similar to those of allopurinol (Fig. 6D). These results indicated that diosmetin and quercetin differentially regulate *in vivo* XOD activity in hyperuricemic mice.

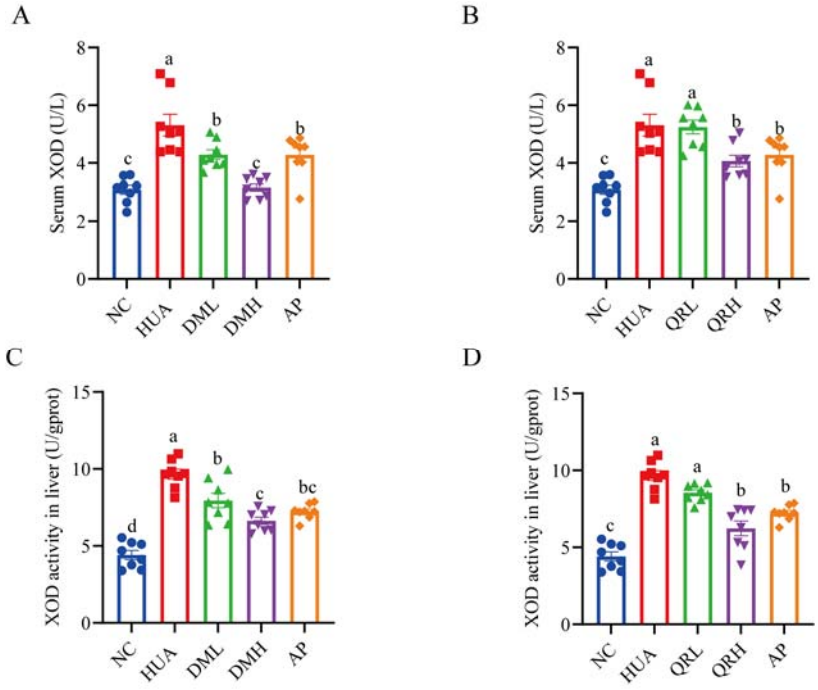

Fig. 6 Effects of diosmetin or quercetin on serum and liver XOD levels in mice with hyperuricemia. (A, B) Serum XOD. (C, D) XOD activity in the liver. Data are presented as the means ± SEMs of biological replicates (n = 8). Differences among experimental groups were analyzed by one-way ANOVA with Tukey's post hoc test. A difference was considered statistically significant when $P < 0.05$. Different letters indicate significant differences between the two groups. **NC**, normal control group; **HUA**, hyperuricemia group (P&F)**; DML**, low-dose diosmetin group (P&F and 10 mg/kg diosmetin); **DMH**, high-dose diosmetin group (P&F and 50 mg/kg diosmetin); **QRL**, low-dose quercetin group (P&F and 10 mg/kg quercetin); **QRH**, high-dose quercetin group (P&F and 50 mg/kg quercetin); **AP**, allopurinol group (P&F and 5 mg/kg AP); XOD, xanthine oxidase; **ANOVA**, analysis of variance.

3.5 Microbial Diversity and Correlation Analyses

To elucidate the effects of diosmetin or quercetin on the gut microbiota in HUA mice, 16S rRNA gene sequencing was conducted to characterize the microbial diversity and community structure. The Sobs (Fig. 7A) and Shannon indices (Fig. 7B) did not significantly differ across the NC, HUA, DML, and DMH groups ($P > 0.05$). Principal component analysis (PCA) (Fig. 7C) and nonmetric multidimensional scaling (NMDS) (Fig. 7D) revealed that the gut microbiota composition in the HUA group differed significantly from that in the NC group ($P < 0.05$), while supplementation with 10 mg/kg diosmetin significantly altered the gut microbiota composition in HUA mice compared with the HUA group ($P < 0.05$). Notably, compared with that in the HUA group, Muribaculaceae abundance was significantly elevated in the 10 mg/kg diosmetin treatment group ($P < 0.05$) (Fig. 7E). Moreover, compared with HUA, 50 mg/kg diosmetin significantly increased the relative abundance of *Lactobacillus johnsonii* ($P < 0.05$) (Fig. 7F), *Alistipes* sp. ($P < 0.05$) (Fig. 7G), and *Odoribacter* sp. ($P < 0.05$) (Fig. 7H) but significantly decreased the abundance of *Desulfovibrio fairfieldensis* ($P < 0.05$) (Fig. 7I). Additionally, to explore the specific microorganisms affected by diosmetin, LEfSe analysis was performed, and the results are presented in Fig. 7J. LEfSe analysis revealed that the NC group harbored different taxa, including *Alistipes* sp.*, Muribaculum* sp., and *Bacteroides caecimuris*, whereas the HUA group was enriched with Ruminococcaceae, *Bilophila* sp.*, Butyribacter* sp.*,* and *Acutalibacter muris.* Treatment with 10 mg/kg diosmetin was distinguished by *Faecalimonas* sp.*, Rikenella* sp.*, GCA-900066575* sp., *Eubacterium siraeum group* sp.*,* and *Clostridia UCG-014* sp.

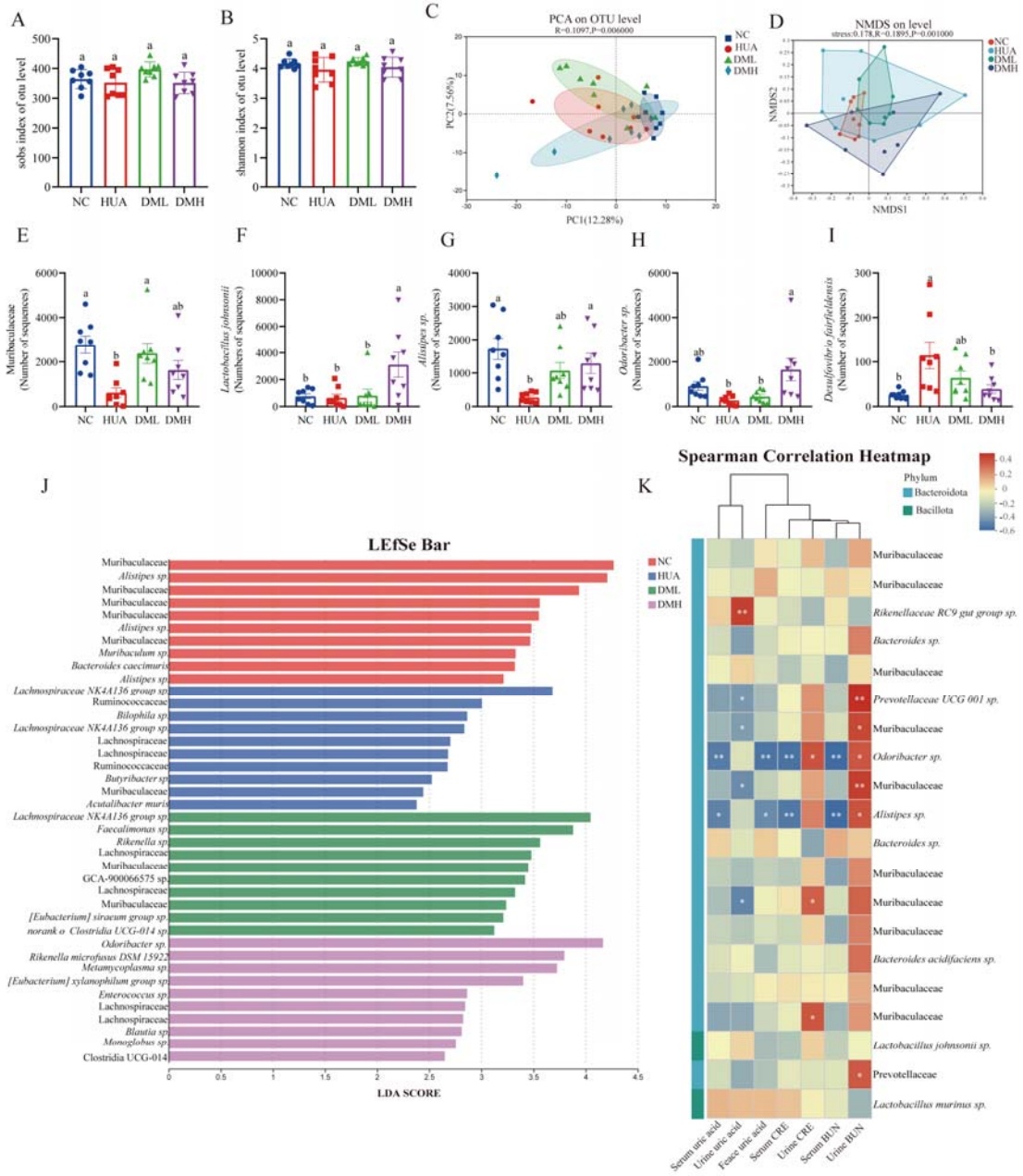

Fig. 7 Effects of diosmetin on the gut microbiota in hyperuricemic mice. (A) Sobs index at the OTU level. (B) Shannon index at the OTU level. (C) Beta diversity based on PCA. (D) NMDS plot of the gut microbiota at the OTU level. (E) Muribaculaceae. (F) *Lactobacillus johnsonii*. (G) *Alistipes* sp. (H) *Odoribacter sp*. (I) *Desulfovibrio fairfieldensis*. (J) Taxonomic cladogram based on LEfSe analysis (bacteria with an LDA score > 4 were considered characteristic taxa). (K) Correlation analysis of the gut microbiota in hyperuricemic mice. Data are shown as the means ± SEMs (n = 8). Differences among experimental groups were analyzed by one-way ANOVA, and Tukey's multiple comparisons test was used for post hoc analysis. A *P* value < 0.05 indicated a significant difference. Distinct letters denote significant differences between the two groups. **NC**, normal control group; **HUA**, hyperuricemia group (P&F)**; DML**, low-dose diosmetin group (P&F and 10 mg/kg diosmetin); **DMH**, high-dose diosmetin group (P&F and 50 mg/kg diosmetin).

In contrast, treatment with 50 mg/kg diosmetin led to enrichment of *Odoribacter* sp.*, Rikenella microfusus DSM 15922, Metamycoplasma* sp.*, Eubacterium xylanophilum group* sp.*, Enterococcus* sp.*, Blautia* sp.*, Monoglobus* sp.*,* and Clostridia UCG-014. To evaluate species-specific associations with UA, CRE, and BUN levels, correlation analyses were performed using a significance threshold of $P < 0.05$, with the results visualized as heatmaps. At the OTU level, *Odoribacter* sp. and *Alistipes* sp. were significantly negatively correlated with the serum and fecal UA levels. For urine UA, negative correlations were observed

with Muribaculaceae and *Prevotellaceae UCG 001* sp., whereas *Rikenellaceae RC9 gut group* sp. was positively correlated. *Odoribacter* sp. and *Alistipes* sp. were negatively correlated with the serum CRE level, whereas Muribaculaceae and *Odoribacter* sp. were positively correlated with the urine CRE level. *Odoribacter* sp. and *Alistipes* sp. were negatively correlated with serum BUN levels, whereas Muribaculaceae, *Odoribacter* sp., *Alistipes* sp., Prevotellaceae, and *Prevotellaceae UCG 001* sp. were positively correlated with urine BUN levels (Fig. 6K).

For quercetin, the Sobs (Fig. 8A) and Shannon indices (Fig. 8B) were not significantly different across the NC, HUA, QRL, and QRH groups ($P > 0.05$). PCA (Fig. 8C) and NMDS (Fig. 8D) revealed that the gut microbiota composition in the HUA group differed significantly from that in the NC group ($P < 0.05$), whereas supplementation with neither 10 mg/kg nor 50 mg/kg quercetin led to significant differences in gut microbiota composition compared with the HUA group ($P > 0.05$). Notably, compared with the HUA group, 10 mg/kg quercetin treatment significantly increased the abundance of *Lactobacillus* sp. ($P < 0.05$) (Fig. 8E) and *Alistipes* sp. ($P < 0.05$) (Fig. 8F) but significantly decreased the abundance of *Desulfovibrionaceae* sp. ($P < 0.05$) (Fig. 8G) and *Desulfovibrio fairfieldensis* ($P < 0.05$) (Fig. 8H). Moreover, compared with HUA, 50 mg/kg quercetin significantly increased the abundance of *Lactobacillus johnsonii* ($P < 0.05$) (Fig. 8I), *Lactobacillus reuteri* ($P < 0.05$) (Fig. 8J), Muribaculaceae ($P < 0.05$) (Fig. 8K), and *Bacteroides thetaiotaomicron* ($P < 0.05$) (Fig. 8L). LEfSe analysis was performed to identify differentially abundant taxa across groups, as depicted in Fig. 8M. At the OTU level, the NC group was dominated by *Rikenella* sp., *Rikenella microfusus DSM 15922*, and the Clostridia vadinBB60 group, whereas the HUA group was significantly enriched with *Lactobacillus murinus*, Ruminococcaceae, *Bilophila* sp., and Lachnospiraceae. Treatment with 10 mg/kg quercetin resulted in differential taxa such as *Prevotellaceae UCG-001* sp., *Bacteroides* sp., *Akkermansia muciniphila, Clostridia UCG-014, Massiliomicrobiota* sp., and the *Eubacterium coprostanoligenes group*. In contrast, treatment with 50 mg/kg quercetin led to enrichment of *Lactobacillus johnsonii, Metamycoplasma* sp., *Lachnoclostridium* sp., and *GCA-900066575* sp. To assess species-specific associations with UA, CRE, and BUN levels, correlation analysis was conducted with a significance threshold of $P < 0.05$, visualized via heatmaps. At the OTU level, Muribaculaceae and *Alistipes* sp. were significantly negatively correlated with serum UA levels. In terms of urine UA levels, a negative correlation was observed with Muribaculaceae, *Odoribacter* sp., and *Alistipes* sp., whereas Muribaculaceae alone exhibited a negative correlation with fecal UA levels. Muribaculaceae was negatively correlated with serum CRE levels, whereas Muribaculaceae, *Odoribacter* sp., and *Alistipes* sp. were positively correlated with urine CRE levels. Muribaculaceae, *Odoribacter* sp., and *Alistipes* sp. were negatively correlated with serum BUN levels but positively associated with urine BUN levels (Fig. 8N).

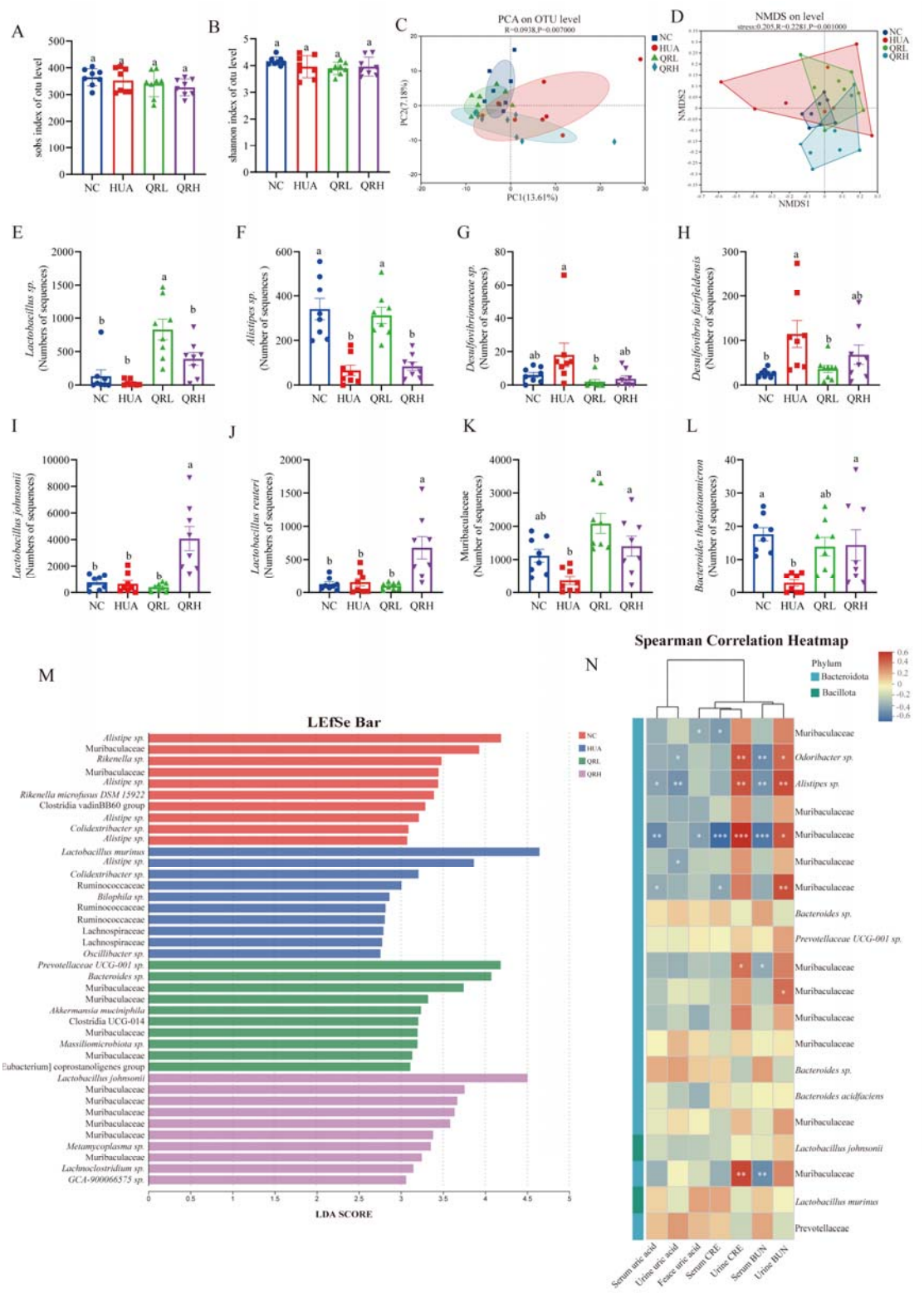

Fig. 8 Effects of quercetin on the gut microbiota of hyperuricemic mice. (A) Sobs index at the OTU level. (B) Shannon index at the OTU level. (C) Beta diversity based on PCA. (D) NMDS plot of the gut microbiota at the OTU level. (E) *Lactobacillus* sp. (F) *Alistipes* sp. (G) *Desulfovibrionaceae* sp. (H) *Desulfovibrio fairfieldensis.* (I) *Lactobacillus johnsonii*. (J) *Lactobacillus reuteri.* (K) Muribaculaceae. (L) *Bacteroides thetaiotaomicron.* (M) Taxonomic cladogram based on LEfSe analysis (bacteria with an LDA score > 4 were considered characteristic taxa). (N) Correlation analysis of the gut microbiota in hyperuricemic mice. Data are shown as the means ± SEMs (n = 8). Differences among experimental groups were analyzed by one-way ANOVA, and Tukey's multiple comparisons test was used for post hoc analysis. A P value < 0.05 indicated a significant difference. Distinct letters denote significant differences between the two groups. **NC**, normal control group; **HUA**, hyperuricemia group (P&F); **QRL**, low-dose quercetin group (P&F and 10 mg/kg quercetin); **QRH**, high-dose quercetin group (P&F and 50 mg/kg quercetin).

3.6 Effects of Diosmetin or Quercetin on Hepatic Injury

To evaluate hepatoprotective effects, the levels of alanine aminotransferase (ALT) and aspartate aminotransferase (AST) were measured. Compared with the NC group, plasma ALT levels were significantly elevated in HUA group mice ($P < 0.05$) (Fig. 9A), which was significantly reversed by treatment with 10 or 50 mg/kg diosmetin ($P < 0.05$) (Fig. 9A). Notably, no reduction in plasma ALT levels was observed in the 50 mg/kg quercetin group compared with the HUA group ($P > 0.05$) (Fig. 9A). Similarly, plasma AST levels were significantly elevated in HUA mice relative to NC mice ($P < 0.05$) (Fig. 9B), and this increase was significantly decreased by 10 or 50 mg/kg diosmetin ($P < 0.05$) (Fig. 9B). In contrast, no reduction in plasma AST levels was observed in the 50 mg/kg quercetin group compared with the HUA group ($P > 0.05$) (Fig. 9B). Additionally, allopurinol treatment did not significantly reduce plasma ALT or AST levels compared with those in the HUA group ($P > 0.05$) (Figs. 9A and 9B). Hepatic ALT levels were lower in HUA mice than in NC mice ($P < 0.05$) (Fig. 9C), whereas treatment with 10 or 50 mg/kg diosmetin significantly increased ALT levels ($P < 0.05$) (Fig. 9C). Conversely, no such increase was observed in the 50 mg/kg quercetin group compared with the HUA group ($P > 0.05$) (Fig. 9C). Similarly, HUA mice presented lower hepatic AST levels than NC mice ($P < 0.05$) (Fig. 9D), and 10 or 50 mg/kg diosmetin significantly increased these levels ($P < 0.05$) (Fig. 9D). However, 50 mg/kg quercetin did not induce a significant increase ($P > 0.05$) (Fig. 9D). Moreover, allopurinol treatment did not significantly increase hepatic ALT or AST levels relative to those in the HUA group ($P > 0.05$) (Figs. 9C and 9D). Furthermore, we predicted the binding activity between diosmetin/quercetin and p38α via molecular docking (Figs. 9E and 9F). Of note, the docking score of diosmetin and p38α was –7.935 (quercetin, –8.760), a weaker binding affinity to p38α (less negative score) and thus a relatively lower hepatotoxic risk for diosmetin. Collectively, based on the current experimental system, the results demonstrate that diosmetin exerts a significant hepatoprotective effect against HUA-induced liver injury by regulating the activity of transaminases in hepatocytes and improving liver function. It also shows a low potential risk of hepatotoxicity, with a superior protective efficacy compared to quercetin and allopurinol.

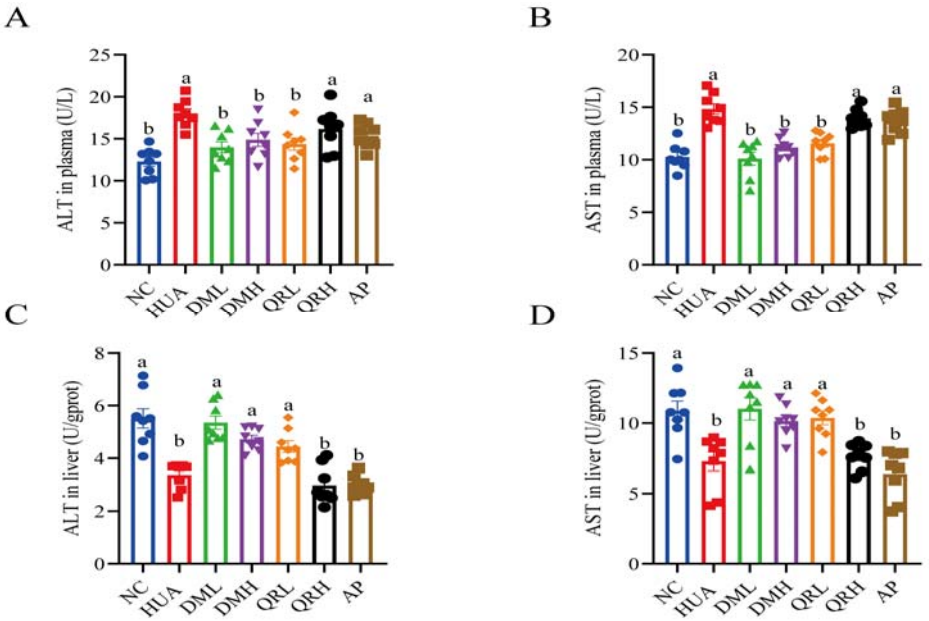

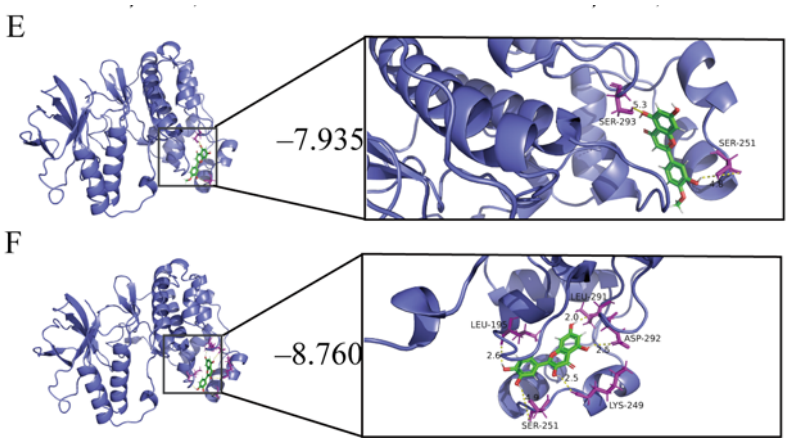

Fig. 9 Effects of diosmetin or quercetin on liver injury in mice. (A) Plasma ALT levels. (B) Plasma AST levels. (C) Liver ALT levels. (D) Liver AST levels. Binding activity of diosmetin (E) and quercetin (F) to p38 MAPK. The docking scores were –7.935 and –8.760, respectively. Data are shown as the means ± SEMs (n = 8). Differences among experimental groups were analyzed by one-way ANOVA, and Tukey's multiple comparisons test was used for post hoc analysis. A *P* value < 0.05 indicated a significant difference. Distinct letters denote significant differences between groups. NC, normal control group; HUA, hyperuricemia group (P&F); DML, low-dose diosmetin group (P&F and 10 mg/kg diosmetin); DMH, high-dose diosmetin group (P&F and 50 mg/kg diosmetin). QRL, low-dose quercetin group (P&F and 10 mg/kg quercetin); QRH, high-dose quercetin group (P&F and 50 mg/kg quercetin); AP, allopurinol group (P&F and 5 mg/kg AP); ALT, alanine aminotransferase; AST, aspartate aminotransferase. The atoms of diosmetin and quercetin are colored as follows: carbon, green; oxygen, red; hydrogen, white. Hydrogen bonds are indicated by yellow dashed lines.

4. Discussion

XOD inhibitors are the main drugs used to treat hyperuricemia. However, these agents consistently cause serious side effects [35]. Currently, the identification and development of safe and effective natural XOD inhibitors are the primary strategies for HUA treatment. In this study, structural characterization revealed that hydroxylation patterns and methoxy substitutions on the B-ring critically governed flavonoid–XOD interactions. Through integrated *in vitro* enzyme kinetics and molecular docking analyses, diosmetin and quercetin were identified as potent XOD inhibitors, both of which exhibited mixed-type inhibition. Moreover, docking analyses based on SWISS-MODEL demonstrated that Asn768 (active site) and Phe1009 (allosteric site) were key residues for diosmetin binding to XOD, whereas Lys771 (active site) and Phe914 (allosteric site) were critical for quercetin binding. Furthermore, *in vivo* validation demonstrated that both diosmetin and quercetin had effects comparable to those of allopurinol in reducing serum UA, inhibiting XOD activity, and even alleviating renal injury in hyperuricemic mice. Moreover, supplementation with diosmetin or quercetin significantly increased the abundance of beneficial bacteria while reducing the abundance of harmful bacteria. Toxicological evaluation demonstrated that, compared with quercetin, diosmetin possessed the potential for reduced toxicity, as evidenced by lower plasma ALT and AST levels and higher molecular docking scores, further supporting its clinical potential. These findings resolve the trade-offs between efficacy and safety of current urate-lowering drugs, providing a promising natural therapeutic strategy for overcoming the limitations of conventional hyperuricemic treatments.

Flavonoids, a class of naturally occurring polyphenolic compounds, are characterized by a C6-C3-C6 skeleton comprising two aromatic rings (A- and B-rings) linked via a heterocyclic pyrone (C-ring) [36]. In recent years, dietary flavonoids have emerged as a research hotspot for managing hyperuricemia due to their

potential XOD-inhibitory activity and favorable safety profile [37]. However, the SAR between dietary flavonoids and XOD remains poorly understood. Our study evaluated the SAR between XOD inhibitory activity and dietary flavonoids. First, the number of hydroxyl substituents on the A- or C-ring positively correlated with XOD inhibitory activity. For the A-ring, more hydroxyl groups enhance potency via strengthened π-π stacking with the hydrophobic pocket of XOD [38]. Specific C-ring hydroxyls form stable hydrogen bonds with XOD residues such as serine and threonine, increasing the binding affinity [39]. For the B-ring, activity rises with increasing hydroxyl numbers initially but then declines with excess due to steric hindrance; for example, quercetin is more potent than myricetin and kaempferol [40]. These data are consistent with our findings, aligning with drug design principles, as observed for febuxostat, where additional hydroxyls reduce efficacy. Second, greater numbers of A-ring methoxy groups strengthened XOD inhibition. As electron-donating substituents, they adjust the flavonoid's electronic density, enhancing π-π stacking with the aromatic residues of XOD [41], and their appropriate steric hindrance stabilizes the binding conformation [42]. Notably, flavonoids with an intermediate number of methoxy groups on the B-ring tend to exhibit increased XOD inhibitory activity, and this phenomenon arises from the combined effects of three factors: optimized hydrophobicity, favorable electronic modulation, and precise steric conformation. An intermediate number of methoxy groups enhances penetration into the XOD active site via balanced hydrophobic interactions [43]. They also fine-tune the electron density on the B-ring, facilitating binding to catalytic residues through hydrogen bonding and electrostatic forces [39]. Additionally, this methoxy group count maintains a spatial structure that avoids steric clashes with the active site [44]. These features are consistent with drug design principles, such as those of COX-2 inhibitors, where optimal polar substituents enhance affinity, but excess polar substituents cause steric clashes [45]. Third, structural modifications of dietary flavonoids, particularly the introduction of glycosyl groups on the A- or C-ring, significantly weaken XOD inhibitory activity. This phenomenon that is attributed to the disrupted planar binding conformation and steric hindrance from glycosyl groups [29], which is consistent with clinically used inhibitors such as allopurinol and febuxostat that lack glycosyl substituents. Thus, avoiding glycosyl groups on the core scaffold is critical for maintaining optimal binding affinity and inhibitory potency. Finally, the C2=C3 double bond in the flavonoid C-ring is crucial for enhancing XOD inhibitory activity, as it restricts the conformational flexibility of the C-ring. This restriction enables precise alignment with key hydrophobic residues in the XOD active site and reinforces π-π stacking interactions with aromatic amino acids, thereby stabilizing the inhibitor–enzyme complex [46]. Consistent with this process, daidzein (with a C2=C3 double bond) inhibits XOD more effectively than its hydrogenated derivative dihydrodaidzein (saturated C2-C3 bond) [47]. Similarly, hydrogenation of the pyran ring double bond in coumarin-based inhibitors weakens XOD binding [39]. These examples highlight that unsaturated structures such as the C2=C3 double bond are critical for the effective binding of diverse XOD inhibitors, offering valuable references for drug design. Overall, optimizing the number and position of hydroxyl and methoxy groups and preserving key unsaturated bonds such as the C2=C3 double bond are critical. These adjustments enhance the binding affinity and inhibitory potency by promoting favorable interactions with

residues in the enzyme's active site. Additionally, these findings underscore that the rational design of XOD inhibitors should prioritize maintaining a planar core structure while avoiding glycosyl substitutions to minimize steric interference.

In XOD inhibitor development, therapeutic strategies balance efficacy and adverse effects. Early competitive inhibitors (allopurinol) act via active-site competition but cause off-target effects such as hypersensitivity due to substrate mimicry [48]. These effects have shifted focus to noncompetitive inhibitors, which bind allosteric sites or enzyme–substrate complexes, reducing side effects. Our finding that diosmetin and quercetin are mixed-type inhibitors is significant, as their broader binding mode lowers off-target risks, which is consistent with studies showing that flavonoids have reduced cytotoxicity [49]. Diosmetin and quercetin exhibit distinct residue-specific binding profiles: Asn768 (active site) and Phe1009 (allosteric site) are pivotal for diosmetin, whereas Lys771 (active site) and Phe914 (allosteric site) are critical for quercetin. These profiles highlight the structural basis underlying their mixed-type inhibition. This divergence underscores how diosmetin's methoxy group substitutions, a key structural distinction from quercetin, modulate its interaction specificity with XOD residues. The hydroxyl group on the flavonoid scaffold likely forms a hydrogen bond with Asn768 in the active site, while the aromatic ring system engages in π–π stacking with Phe1009 at the allosteric pocket. The methoxy substitution may further enhance this stacking interaction by increasing the electron density of the aromatic system, thereby stabilizing the inhibitor–enzyme complex [50]. Such residue-selective interactions not only explain the differential binding affinities of these flavonoids but also emphasize the importance of tailoring substituent patterns to engage both active and allosteric residues. This strategy could optimize mixed-type inhibitory potency in XOD-targeting drug design.

Current first-line urate-lowering medications, such as allopurinol and febuxostat, have demonstrated efficacy in managing hyperuricemia [5]. However, accumulating evidence indicates that these agents may inadvertently disrupt gut microbial homeostasis, potentially contributing to suboptimal therapeutic efficacy and adverse effects [51]. Previous research has shown that prolonged administration of allopurinol reduces the abundance of SCFA-producing bacteria (*Lactobacillus*) while increasing that of conditional pathogens (Desulfovibrionaceae) in the gut microbiota [20]. Notably, the loss of beneficial Lactobacillus species (*Lactobacillus johnsonii, Lactobacillus reuteri*) weakens intestinal barrier integrity, promotes systemic inflammation, and suppresses the NOD-like receptor family pyrin domain containing 3 (NLRP3) inflammasome [52, 53]. These processes lead to elevated Interleukin-1 beta (IL-1β) and Tumor Necrosis Factor-alpha (TNF-α), which inhibit renal uric acid excretion by down regulating ATP-binding cassette sub-family G member 2 (ABCG2)/Urate transporter 1 (URAT1) transporters [54]. Desulfovibrionaceae generate hydrogen sulfide (H_2S) and lipopolysaccharides (LPS), which activate the Toll-like receptor 4 (TLR4)/ Nuclear factor kappa-light-chain-enhancer of activated B cells (NF-κB) pathways to amplify proinflammatory cytokine release and promote intestinal permeability, thereby facilitating endotoxin translocation and systemic low-grade inflammation [55]. This dysbiosis may contribute to the reduced therapeutic efficacy of allopurinol. In our study, diosmetin supplementation increased the abundance of beneficial bacteria (*Lactobacillus johnsonii*,

Muribaculaceae, *Alistipes* sp., and *Odoribacter* sp.) and reduced the abundance of harmful bacteria (*Desulfovibrio fairfieldensis*). These beneficial modifications to the gut microbiota might enable diosmetin to avoid effects similar to those of allopurinol, which was conducive to its long-term administration. Additionally, Muribaculaceae, *Alistipes* sp., and *Odoribacter sp*. were correlated with UA, CRE, and BUN levels, whereas Prevotellaceae and *Prevotellaceae UCG-001* sp. were correlated with urine UA and urine BUN levels. Specifically, Muribaculaceae, a dominant family in the murine and human gut microbiota, has been reported to participate in purine metabolism by modulating the production of SCFAs and bile acid metabolites, which may directly promote urate excretion through renal and intestinal pathways [56]. Similarly, *Alistipes* sp. has been associated with reduced systemic inflammation via the inhibition of proinflammatory cytokine (e.g., TNF-α) secretion, potentially mitigating urate-induced renal and joint tissue damage [57]. Similarly, the *Odoribacter* sp., particularly *Odoribacter splanchnicus*, has been identified as a key target of Bacillus subtilis-fermented Astragalus membranaceus (BFA) in gut microbiota regulation [58]. This bacterial species, which has been shown to exert anti-inflammatory effects, protect the intestinal barrier, and promote urate excretion via SCFAs production, has been found to thereby contribute to the amelioration of hyperuricemia and associated renal injury [59]. Moreover, Prevotellaceae species may mitigate renal injury by balancing nitrogen metabolism [60]. Moreover, *Prevotellaceae UCG-001* sp. may increase urate excretion by metabolizing purine precursors [24]. In comparison, quercetin supplementation increased the abundance of beneficial bacteria (*Lactobacillus johnsonii, Lactobacillus reuteri, Lactobacillus* sp.*,* Muribaculaceae, *Alistipes* sp., *Bacteroides thetaiotaomicron*) and reduced the abundance of harmful bacteria (*Desulfovibrionaceae* sp., *Desulfovibrio fairfieldensis*). Additionally, similar to diosmetin, Muribaculaceae, *Alistipes* sp., and *Odoribacter* sp. were correlated with UA, CRE, and BUN levels, suggesting that this might be one mechanism by which quercetin alleviated HUA via microbiota regulation. Overall, diosmetin and quercetin may reduce uric acid and protect the kidney by improving the gut microbiota; however, the specific underlying mechanisms remain to be further investigated. These findings highlight that natural product-derived XOD inhibitors, by leveraging microbiota-mediated multitarget regulation, hold greater therapeutic potential than existing pharmaceuticals.

[61]. For example, febuxostat, despite its potent XOD inhibitory activity, has been associated with rare but severe liver injury, including elevated serum transaminases and, in extreme cases, fulminant hepatitis, leading to black box warnings in some regions [62]. Similarly, allopurinol, although widely used, can induce idiosyncratic hepatotoxicity, particularly in patients with preexisting liver dysfunction, characterized by hepatocellular necrosis and cholestasis [63]. These adverse effects underscore the urgency of developing XOD inhibitors with improved hepatic safety profiles. In contrast, our findings revealed that diosmetin has relatively lower potential hepatotoxicity than quercetin. This is supported by the restoration of plasma ALT and AST levels (toward normal ranges) in the diosmetin-treated group, coupled with molecular docking results indicating a weaker binding affinity of diosmetin for p38α. This favorable safety profile may be attributed to multiple structural and mechanistic features. Structurally, diosmetin contains a methoxy group at the 4'-

position of the B-ring, whereas quercetin bears a hydroxyl group at this site. Previous studies have demonstrated that methoxy substitutions in flavonoids can reduce electrophilicity, thereby mitigating oxidative stress-induced liver damage—an effect linked to the hydroxyl group-mediated generation of reactive oxygen species (ROS) in hepatocytes [64]. Additionally, a weaker interaction with p38α was observed in docking studies. This finding is consistent with a report by Goettert et al. [65], which indicates that p38α activation acts as a key driver of hepatocyte apoptosis and inflammation in drug-induced liver injury. Specifically, reduced binding to this kinase may thus dampen proinflammatory signaling cascades in hepatic tissues. Collectively, these findings suggest that the structural attributes and selective kinase-binding properties of diosmetin may contribute to its relatively lower potential hepatotoxicity, supporting its potential as a safer alternative to both conventional XOD inhibitors and certain natural product derivatives under the tested conditions.

While our study demonstrated the potential therapeutic benefits of diosmetin and quercetin, several limitations must be considered. First, optimal dietary flavonoid intake levels and consumption patterns for different populations (by age, sex, or underlying conditions) are undefined. Our study did not address how intake amount/frequency affects efficacy or group-specific responses, highlighting the need for population studies to establish practical guidelines. Second, the long-term effects of dietary flavonoids on the gut microbiota and overall health need to be further investigated. While our study revealed positive modulation of the microbiota, the long-term impact on gut health and potential side effects are still unknown. More studies are necessary to fully understand the safety and efficacy of dietary flavonoids in humans. Therefore, further research is needed to support the use of dietary flavonoids as supplements.

5. Conclusion

In conclusion, our study elucidates the SAR between dietary flavonoids and XOD activity. It also preliminary verifies that diosmetin and quercetin, as potent XOD-inhibiting dietary flavonoids, hold potential application value in the prevention and management of hyperuricemia through dietary modulation. Notably, diosmetin's capacity to regulate gut microbiota homeostasis and mitigate potential hepatotoxicity (relative to quercetin) renders it a promising natural dietary component for in-depth investigation. These findings thus lay a vital theoretical basis for subsequent research on natural product-based targeted nutritional strategies for hyperuricemia.

Funding

This work was supported by the National Key Research and Development Program of China (2024YFC3506304).

Conflict of interest statement

The authors declare that there are no conflicts of interest associated with this study.

Ethical approval

This paper does not involve clinical studies or data. All animal protocols followed international ethical guidelines and were approved by the Institutional Animal Care and Use Committee of Shandong University of Technology (Permission No. YLX202403012). All procedures were conducted in accordance with the ARRIVE 2.0 guidelines. Every effort was made to minimize animal suffering and to reduce the number of animals used.

Supporting Information statement

Supplementary Materials for this article can be found online.

Data availability

All raw sequencing data have been deposited in the NCBI Sequence Read Archive (SRA) under project PRJNA1294550. All other data needed to evaluate the conclusions in the paper are presented in the manuscript and the Supplementary Materials. Additional information is available from the corresponding authors upon reasonable request

References

[1] C. Hou, D. Liu, M. Wang, et al., Novel xanthine oxidase-based cell model using HK-2 cell for screening antihyperuricemic functional compounds, Free Radic Biol Med. 136 (2019) 135-145. https://doi.org/10.1016/j.freeradbiomed.2019.04.007.

[2] M. Dehlin, L. Jacobsson, E. Roddy, Global epidemiology of gout: prevalence, incidence, treatment patterns and risk factors, Nat Rev Rheumatol. 16 (2020) 380-390. https://doi.org/10.1038/s41584-020-0441-1.

[3] L. Wang, S. Yue, J. Liao, et al., Integrating genomics and artificial intelligent tools to unlock the safety and uricolytic activities of promising purinolytic Lactobacillus plantarum L123, Journal of Future Foods. (2025) https://doi.org/10.1016/j.jfutfo.2025.04.016.

[4] P. Lin, Z. Chen, J. Lin, Therapeutic drugs of gout: The progress in target selection, Int. J. Rheum. Dis. 27 (2024) e15022. https://doi.org/10.1111/1756-185x.15022.

[5] W.B. White, K.G. Saag, M.A. Becker, et al., Cardiovascular Safety of Febuxostat or Allopurinol in Patients with Gout, The New England journal of medicine. 378 (2018) 1200-1210. https://doi.org/10.1056/NEJMoa1710895.

[6] R. Alten, M. Mischkewitz, S. Nitschmann, [Febuxostat or allopurinol in patients with gout : Cardiovascular Safety of Febuxostat and Allopurinol in Patients with Gout and Cardiovascular Morbidities (CARES)], Internist (Berl.). 61 (2020) 530-532. https://doi.org/10.1007/s00108-020-00766-4.

[7] W. Yaseen, B. Auguste, J. Zipursky, Allopurinol hypersensitivity syndrome, Cmaj. 195 (2023) E483. https://doi.org/10.1503/cmaj.221575.

[8] T.A. Johnson, N. Kamatani, M. Kuwabara, Xanthine Oxidase Inhibitor Withdrawal Syndrome? Comment on the Article by Choi et al, Arthritis & rheumatology (Hoboken, N.J.). 71 (2019) 1966-1967. https://doi.org/10.1002/art.41066.

[9] W. Li, H. Chen, B. Xu, et al., Research progress on classification, sources and functions of dietary polyphenols for prevention and treatment of chronic diseases, Journal of Future Foods. 3 (2023) 289-305. https://doi.org/10.1016/j.jfutfo.2023.03.001.

[10] C.-H. Wu, T.-M. Shieh, K.-L. Wang, et al., Quercetin, a main flavonoid in onion, inhibits the PGF2α-induced uterine contraction in vitro and in vivo, Journal of Functional Foods. 19 (2015) 495-504. https://doi.org/10.1016/j.jff.2015.09.028.

[11] Z. Sun, K. Liu, C. Liang, et al., Diosmetin as a promising natural therapeutic agent: In vivo, in vitro mechanisms, and clinical studies, Phytother. Res. 38 (2024) 3660-3694. https://doi.org/10.1002/ptr.8214.

[12] M. Minaiyan, S.M. Ghanadian, M. Hossaini, Protective Effect of Apium graveolens L. (Celery) Seeds Extracts and Luteolin on Acetic Acid-Induced Colitis in Rats, Int. J. Prev. Med. 12 (2021) 100. https://doi.org/10.4103/ijpvm.IJPVM_651_20.

[13] D. Geng, R. Wang, Y. Zhang, et al., A 13-LOX participates in the biosynthesis of JAs and is related to the accumulation of baicalein and wogonin in Scutellaria baicalensis, Frontiers in plant science. 14 (2023) 1204616.

https://doi.org/10.3389/fpls.2023.1204616.

[14] F. Liu, Y. Bai, Y. Wan, et al., Mechanism of flavonoids in the treatment of gouty arthritis (Review), Mol. Med. Rep. 30 (2024) https://doi.org/10.3892/mmr.2024.13256.

[15] Y. Wang, X.J. Liu, J.B. Chen, et al., Citrus flavonoids and their antioxidant evaluation, Crit. Rev. Food Sci. Nutr. 62 (2022) 3833-3854. https://doi.org/10.1080/10408398.2020.1870035.

[16] T. Vezza, E. Guillamón, J. García-García, et al., LDL-Cholesterol-Lowering Effects of a Dietary Supplement Containing Onion and Garlic Extract Used in Healthy Volunteers, Nutrients. 16 (2024) https://doi.org/10.3390/nu16162811.

[17] B.H. Parmenter, A.S. Thompson, N.P. Bondonno, et al., High diversity of dietary flavonoid intake is associated with a lower risk of all-cause mortality and major chronic diseases, Nature food. 6 (2025) 668-680. https://doi.org/10.1038/s43016-025-01176-1.

[18] H. Alkhalidy, Y. Wang, D. Liu, Dietary Flavonoids in the Prevention of T2D: An Overview, Nutrients. 10 (2018) 438. https://doi.org/10.3390/nu10040438.

[19] S. Lin, T. Zhang, L. Zhu, et al., Characteristic dysbiosis in gout and the impact of a uric acid-lowering treatment, febuxostat on the gut microbiota, J Genet Genomics. 48 (2021) 781-791. https://doi.org/10.1016/j.jgg.2021.06.009.

[20] C. Ni, X. Li, L. Wang, et al., Lactic acid bacteria strains relieve hyperuricaemia by suppressing xanthine oxidase activity via a short-chain fatty acid-dependent mechanism, Food Funct. 12 (2021) 7054-7067. https://doi.org/10.1039/d1fo00198a.

[21] X. Lin, M. Wang, Z. He, et al., Gut microbiota mediated the therapeutic efficiency of Simiao decoction in the treatment of gout arthritis mice, BMC complementary medicine and therapies. 23 (2023) 206. https://doi.org/10.1186/s12906-023-04042-4.

[22] U. Wegmann, P. Louis, A. Goesmann, et al., Complete genome of a new Firmicutes species belonging to the dominant human colonic microbiota ('Ruminococcus bicirculans') reveals two chromosomes and a selective capacity to utilize plant glucans, Environ Microbiol. 16 (2014) 2879-2890. https://doi.org/10.1111/1462-2920.12217.

[23] Z.X. Zhao, X.H. Tang, S.L. Jiang, et al., Astragaloside IV improves the pharmacokinetics of febuxostat in rats with hyperuricemic nephropathy by regulating urea metabolism in gut microbiota, Front. Pharmacol. 13 (2022) 1031509. https://doi.org/10.3389/fphar.2022.1031509.

[24] F. Zhao, N. Tie, L.Y. Kwok, et al., Baseline gut microbiome as a predictive biomarker of response to probiotic adjuvant treatment in gout management, Pharmacol Res. 209 (2024) 107445. https://doi.org/10.1016/j.phrs.2024.107445.

[25] A.E. Lindell, M. Zimmermann-Kogadeeva, K.R. Patil, Multimodal interactions of drugs, natural compounds and pollutants with the gut microbiota, Nature reviews. Microbiology. 20 (2022) 431-443. https://doi.org/10.1038/s41579-022-00681-5.

[26] L. Wang, M. Li, Y. Gu, et al., Dietary flavonoids-microbiota crosstalk in intestinal inflammation and carcinogenesis, J. Nutr. Biochem. 125 (2024) 109494. https://doi.org/10.1016/j.jnutbio.2023.109494.

[27] Y.-F. Liu, N. Ling, B. Zhang, et al., Flavonoid-Rich mulberry leaf extract modulate lipid metabolism, antioxidant capacity, and gut microbiota in high-fat diet-induced obesity: potential roles of FGF21 and SOCS2, Food & Medicine Homology. 1 (2024) 9420016. https://doi.org/10.26599/FMH.2024.9420016.

[28] Z. Shou-huan, Y. Hui, S.H.I. Guan-ying, et al., Optimization of the three natural products' inhibitory effect on xanthine oxidase by response surface methodology, Science and Technology of Food Industry. 39 (2018) 230-234,318. https://www.spgykj.com/en/article/id/102ac3d9-b14a-408c-a257-04e4abf09cbd

[29] Y. Yu, Y. Xiong, S. Tong, et al., Inhibitory Activity of Quercetin, Rutin, and Hyperoside against Xanthine Oxidase: Kinetics, Fluorescence, and Molecular Docking, Curr Pharm Biotechnol. 26 (2025) 513-524. https://doi.org/10.2174/0113892010297269240427055003.

[30]O.S. Ajala, A.O. Ayeleso, M. Owolabi, et al., Xanthine oxidase inhibitory potentials of flavonoid aglycones of Tribulus terrestris: in vivo, in silico and in vitro studies, Future Journal of Pharmaceutical Sciences. 8 (2022) 58. https://doi.org/10.1186/s43094-022-00448-y.

[31] B. González-Terán, N. Matesanz, I. Nikolic, et al., p38γ and p38δ reprogram liver metabolism by modulating neutrophil infiltration, The EMBO journal. 35 (2016) 536-552. https://doi.org/10.15252/embj.201591857.

[32] Y. Xiao, J. Wang, W. Yan, et al., p38α MAPK antagonizing JNK to control the hepatic fat accumulation in pediatric patients onset intestinal failure, Cell death & disease. 8 (2017) e3110. https://doi.org/10.1038/cddis.2017.523.

[33] G.P. Sreekanth, A. Chuncharunee, A. Sirimontaporn, et al., SB203580 Modulates p38 MAPK Signaling and Dengue Virus-

Induced Liver Injury by Reducing MAPKAPK2, HSP27, and ATF2 Phosphorylation, PloS one. 11 (2016) e0149486. https://doi.org/10.1371/journal.pone.0149486.

[34] F. Li, Y.Z. Dong, D. Zhang, et al., Molecular mechanisms involved in drug-induced liver injury caused by urate-lowering Chinese herbs: A network pharmacology study and biology experiments, PloS one. 14 (2019) e0216948. https://doi.org/10.1371/journal.pone.0216948.

[35] Y.-X. Wang, X.-L. Chen, K. Zhou, et al., Fucoidan dose-dependently alleviated hyperuricemia and modulated gut microbiota in mice, Food & Medicine Homology. (2025) https://doi.org/10.26599/FMH.2026.9420095.

[36] T.Y. Wang, Q. Li, K.S. Bi, Bioactive flavonoids in medicinal plants: Structure, activity and biological fate, Asian J Pharm Sci. 13 (2018) 12-23. https://doi.org/10.1016/j.ajps.2017.08.004.

[37] Z. Ullah, P. Yue, G. Mao, et al., A comprehensive review on recent xanthine oxidase inhibitors of dietary based bioactive substances for the treatment of hyperuricemia and gout: Molecular mechanisms and perspective, Int. J. Biol. Macromol. 278 (2024) 134832. https://doi.org/10.1016/j.ijbiomac.2024.134832.

[38] B.B. Roba, A.B. Umar, Investigating the potential of novel antioxidant flavonoids: a comprehensive study of drug-likeness, molecular docking, pharmacokinetics, and DFT analysis, Future Journal of Pharmaceutical Sciences. 11 (2025) 84. https://doi.org/10.1186/s43094-025-00837-z.

[39] M. Yuan, Y. Liu, A. Xiao, et al., The interaction of dietary flavonoids with xanthine oxidase in vitro: molecular property-binding affinity relationship aspects, RSC Adv. 9 (2019) 10781-10788. https://doi.org/10.1039/c8ra09926j.

[40] X.Y. Li, J. Shang, X.J. Wang, et al., Bifidobacterium longum JBLC-141 alleviates hypobaric hypoxia-induced intestinal barrier damage by attenuating inflammatory responses and oxidative stress, Front Microbiol. 15 (2024) 1501999. https://doi.org/10.3389/fmicb.2024.1501999.

[41] M. Aidiel, M. Abdul Mutalib, R. Ramasamy, et al., Mechanistic Insights into the Anticancer Potential of Methoxyflavones Analogs: A Review, Molecules (Basel, Switzerland). 30 (2025) 346. https://doi.org/10.3390/molecules30020346.

[42] D. Navarro-Acosta, L. Coba-Jiménez, W. León-Sotomayor, et al., Integrative computational approach for hyperuricemia treatment: 3D QSAR, molecular docking and dynamics of flavonoid analogues as xanthine oxidase inhibitors, Journal of Molecular Structure. 1322 (2025) 140395. https://doi.org/10.1016/j.molstruc.2024.140395.

[43] S. Pal, C. Saha, A review on structure-affinity relationship of dietary flavonoids with serum albumins, J Biomol Struct Dyn. 32 (2014) 1132-1147. https://doi.org/10.1080/07391102.2013.811700.

[44] J. Wen, Y. Liao, D. Gong, et al., Effects of unsaturated fatty acids on the interaction between phloretin and xanthine oxidase: Inhibitory activity, binding ability and molecular structure, Food Bioscience. 68 (2025) 106669. https://doi.org/10.1016/j.fbio.2025.106669.

[45] R. Sardella, F. Ianni, A. Di Michele, et al., Enantioresolution and stereochemical characterization of two chiral sulfoxides endowed with COX-2 inhibitory activity, Chirality. 29 (2017) 536-540. https://doi.org/10.1002/chir.22724.

[46] K. Li, Y. Wang, W. Liu, et al., Structure-Activity Relationships and Changes in the Inhibition of Xanthine Oxidase by Polyphenols: A Review, Foods (Basel, Switzerland). 13 (2024) 2365. https://doi.org/10.3390/foods13152365.

[47] Y.Z. Zheng, G. Deng, D.F. Chen, et al., The influence of C2C3 double bond on the antiradical activity of flavonoid: Different mechanisms analysis, Phytochemistry. 157 (2019) 1-7. https://doi.org/10.1016/j.phytochem.2018.10.015.

[48] L.K. Stamp, P.T. Chapman, Allopurinol hypersensitivity: Pathogenesis and prevention, Best Pract Res Clin Rheumatol. 34 (2020) 101501. https://doi.org/10.1016/j.berh.2020.101501.

[49] I. Santos, A. Sousa, A. Vale, et al., Protective effects of flavonoids against silver nanoparticles-induced toxicity, Arch Toxicol. (2025) https://doi.org/10.1007/s00204-025-04068-2.

[50] M.D. Sacco, K.G. Kroeck, M.T. Kemp, et al., Influence of the α-Methoxy Group on the Reaction of Temocillin with Pseudomonas aeruginosa PBP3 and CTX-M-14 β-Lactamase, Antimicrob. Agents Chemother. 64 (2019) https://doi.org/10.1128/aac.01473-19.

[51] A.K. Singh, S.S.K. Durairajan, A. Iyaswamy, et al., Elucidating the role of gut microbiota dysbiosis in hyperuricemia and gout: Insights and therapeutic strategies, World J. Gastroenterol. 30 (2024) 4404-4410. https://doi.org/10.3748/wjg.v30.i40.4404.

[52] Y.J. Zou, J.J. Xu, X. Wang, et al., Lactobacillus johnsonii L531 Ameliorates Escherichia coli-Induced Cell Damage via Inhibiting NLRP3 Inflammasome Activity and Promoting ATG5/ATG16L1-Mediated Autophagy in Porcine Mammary

Epithelial Cells, Vet Sci. 7 (2020) https://doi.org/10.3390/vetsci7030112.

[53] Y. Zhang, Y. Li, X. Wang, et al., Lactobacillus Plantarum NC8 and its metabolite acetate alleviate type 1 diabetes via inhibiting NLRP3, Microb. Pathog. 182 (2023) 106237. https://doi.org/10.1016/j.micpath.2023.106237.

[54] H. Wu, Y. Wang, Z. Ren, et al., Overnutrition-induced gout: An immune response to NLRP3 inflammasome dysregulation by XOD activity increased in quail, Front. Immunol. 13 (2022) 1074867. https://doi.org/10.3389/fimmu.2022.1074867.

[55] S.B. Singh, A. Carroll-Portillo, H.C. Lin, Desulfovibrio in the Gut: The Enemy within?, Microorganisms. 11 (2023) 1772. https://doi.org/10.3390/microorganisms11071772.

[56] Y. Lee, P. Werlinger, J.W. Suh, et al., Potential Probiotic Lacticaseibacillus paracasei MJM60396 Prevents Hyperuricemia in a Multiple Way by Absorbing Purine, Suppressing Xanthine Oxidase and Regulating Urate Excretion in Mice, Microorganisms. 10 (2022) 851. https://doi.org/10.3390/microorganisms10050851.

[57] J. Fu, G. Li, X. Li, et al., Gut commensal Alistipes as a potential pathogenic factor in colorectal cancer, Discover oncology. 15 (2024) 473. https://doi.org/10.1007/s12672-024-01393-3.

[58] R. Wang, F. Lin, C. Ye, et al., Multi-omics analysis reveals therapeutic effects of Bacillus subtilis-fermented Astragalus membranaceus in hyperuricemia via modulation of gut microbiota, Food Chem. 399 (2023) 133993. https://doi.org/10.1016/j.foodchem.2022.133993.

[59] J. Li, J. Xu, X. Guo, et al., Odoribacter splanchnicus-A Next-Generation Probiotic Candidate, Microorganisms. 13 (2025) 815. https://doi.org/10.3390/microorganisms13040815.

[60] M. Asgharian, P. Gholizadeh, H. Samadi Kafil, et al., Correlation of inflammatory biomarkers with the diversity of Bacteroidaceae, Bifidobacteriaceae, Prevotellaceae and Lactobacillaceae families in the intestinal microbiota of patients with end stage renal disease, Adv. Med. Sci. 67 (2022) 304-310. https://doi.org/10.1016/j.advms.2022.07.004.

[61] C. Zhang, G. Zhang, J. Pan, et al., Galangin competitively inhibits xanthine oxidase by a ping-pong mechanism, Food Res. Int. 89 (2016) 152-160. https://doi.org/10.1016/j.foodres.2016.07.021.

[62] M. Bohm, R. Vuppalanchi, N. Chalasani, Febuxostat-induced acute liver injury, Hepatology (Baltimore, Md.). 63 (2016) 1047-1049. https://doi.org/10.1002/hep.28403.

[63] R.J. Fontana, Y.J. Li, E. Phillips, et al., Allopurinol hepatotoxicity is associated with human leukocyte antigen Class I alleles, Liver Int. 41 (2021) 1884-1893. https://doi.org/10.1111/liv.14903.

[64] K. Jomova, S.Y. Alomar, R. Valko, et al., Flavonoids and their role in oxidative stress, inflammation, and human diseases, Chem. Biol. Interact. 413 (2025) 111489. https://doi.org/10.1016/j.cbi.2025.111489.

[65] M. Goettert, V. Schattel, P. Koch, et al., Biological evaluation and structural determinants of p38α mitogen-activated-protein kinase and c-Jun-N-terminal kinase 3 inhibition by flavonoids, Chembiochem : a European journal of chemical biology. 11 (2010) 2579-2588. https://doi.org/10.1002/cbic.201000487.

[66] G.E. Batiha, A.M. Beshbishy, M. Ikram, et al., The Pharmacological Activity, Biochemical Properties, and Pharmacokinetics of the Major Natural Polyphenolic Flavonoid: Quercetin, Foods (Basel, Switzerland). 9 (2020) https://doi.org/10.3390/foods9030374.

[67] A. Sato, T. Zhang, L. Yonekura, et al., Antiallergic activities of eleven onions (Allium cepa) were attributed to quercetin 4′-glucoside using QuEChERS method and Pearson's correlation coefficient, Journal of Functional Foods. 14 (2015) 581-589. https://doi.org/10.1016/j.jff.2015.02.029.

[68]B. Singh, B.C. Semwal, S. Singh, Recent Advances in Diosmetin: Pharmacological, Pharmacokinetic, and Toxicological Profile, Curr. Top. Med. Chem. 25 (2025) 2100-2113. https://doi.org/10.2174/0115680266355377250213054844.

[69] H.-Y. Liang, M. Guan, T.-H. Li, et al., Critical review on biological effect and mechanisms of diterpenoids in Rosmarinus officinalis, Food & Medicine Homology. 2 (2025) 9420021. https://doi.org/10.26599/FMH.2025.9420021.

[70] B.L. Freeman, D.L. Eggett, T.L. Parker, Synergistic and antagonistic interactions of phenolic compounds found in navel oranges, J. Food Sci. 75 (2010) C570-576. https://doi.org/10.1111/j.1750-3841.2010.01717.x.

[71] Q. Liu, L. Li, H. Cheng, et al., The basic helix-loop-helix transcription factor TabHLH1 increases chlorogenic acid and luteolin biosynthesis in Taraxacum antungense Kitag, Horticulture research. 8 (2021) 195. https://doi.org/10.1038/s41438-021-00630-y.

[72] H.N. Choi, M.J. Kang, S.J. Lee, et al., Ameliorative effect of myricetin on insulin resistance in mice fed a high-fat, high-sucrose

diet, Nutr. Res. Pract. 8 (2014) 544-549. https://doi.org/10.4162/nrp.2014.8.5.544.

[73] T. Carević, S. Kolarević, M.K. Kolarević, et al., Citrus flavonoids diosmin, myricetin and neohesperidin as inhibitors of Pseudomonas aeruginosa: Evidence from antibiofilm, gene expression and in vivo analysis, Biomed. Pharmacother. 181 (2024) 117642. https://doi.org/10.1016/j.biopha.2024.117642.

[74] Q. Zhang, Y. Zhao, M. Zhang, et al., Recent advances in research on vine tea, a potential and functional herbal tea with dihydromyricetin and myricetin as major bioactive compounds, Journal of pharmaceutical analysis. 11 (2021) 555-563. https://doi.org/10.1016/j.jpha.2020.10.002.

[75] N. Castillo-Muñoz, S. Gómez-Alonso, E. García-Romero, et al., Flavonol profiles of Vitis vinifera red grapes and their single-cultivar wines, J. Agric. Food Chem. 55 (2007) 992-1002. https://doi.org/10.1021/jf062800k.

[76] K. Gohel, K. Patel, P. Shah, et al., Box—Behnken Design-Assisted Optimization for Simultaneous Estimation of Quercetin, Kaempferol, and Keto-β-Boswellic Acid by High-Performance Thin-Layer Chromatography Method, J. Planar. Chromatogr. Mod. TLC. 31 (2018) 318-326. https://doi.org/10.1556/1006.2018.31.4.7.

[77] S. Latif, M. Sameeullah, H.Q. Abbasi, et al., Broccoli (Brassica oleracea var. italica) leaves exhibit significant antidiabetic potential in alloxan-induced diabetic rats: the putative role of ABC vacuolar transporter for accumulation of Quercetin and Kaempferol, Front. Pharmacol. 15 (2024) 1421131. https://doi.org/10.3389/fphar.2024.1421131.

[78] A. Ghasemzadeh, H.Z. Jaafar, A. Rahmat, Identification and concentration of some flavonoid components in Malaysian young ginger (Zingiber officinale Roscoe) varieties by a high performance liquid chromatography method, Molecules (Basel, Switzerland). 15 (2010) 6231-6243. https://doi.org/10.3390/molecules15096231.

[79] X. Liu, S. Jiang, Y. Li, et al., CsHCT synthesizes acylated flavonoid, kaempferol-3-O-(6″-p-coumaroyl)-glucoside, to enhance cold resistance in tea plants (Camellia sinensis), J. Integr. Plant Biol. (2025) https://doi.org/10.1111/jipb.70055.

[80] S. Mohanlal, R. Parvathy, V. Shalini, et al., Isolation, characterization and quantification of tricin and flavonolignans in the medicinal rice Njavara (Oryza sativa L.), as compared to staple varieties, Plant Foods Hum. Nutr. (Dordr.). 66 (2011) 91-96. https://doi.org/10.1007/s11130-011-0217-5.

[81] Y.S. Lee, H. Jeon, Y.M. Her, et al., Lomens-P0 (mixed extracts of Hordeum vulgare and Chrysanthemum zawadskii) regulate the expression of factors affecting premenstrual syndrome symptoms, Nutr. Res. Pract. 15 (2021) 715-731. https://doi.org/10.4162/nrp.2021.15.6.715.

[82] J. Rencoret, G. Marques, M.J. Rosado, et al., Variations in the composition and structure of the lignins of oat (Avena sativa L.) straws according to variety and planting season, Int. J. Biol. Macromol. 242 (2023) 124811. https://doi.org/10.1016/j.ijbiomac.2023.124811.

[83] X. Liu, F. Tian, Y. Tian, et al., Isolation and Identification of Potential Allelochemicals from Aerial Parts of Avena fatua L. and Their Allelopathic Effect on Wheat, J. Agric. Food Chem. 64 (2016) 3492-3500. https://doi.org/10.1021/acs.jafc.5b05498.

[84] R. Liu, H. Li, N. Wei, et al., Simultaneous determination of two galangin metabolites from Alpinia Officinarum Hance in rat plasma by UF LC-MS/MS and its application in pharmacokinetics study, PeerJ. 9 (2021) e11041. https://doi.org/10.7717/peerj.11041.

[85] L. Vazquez, D. Armada, M. Celeiro, et al., Evaluating the Presence and Contents of Phytochemicals in Honey Samples: Phenolic Compounds as Indicators to Identify Their Botanical Origin, Foods (Basel, Switzerland). 10 (2021) https://doi.org/10.3390/foods10112616.

[86] J. Liu, S. Guo, J. Gong, et al., Identification of the Anti-ischemia-reperfusion Injury Effect of Baicalein from Scutellaria baicalensis Georgi in Liver Transplantation, Curr. Med. Chem. 32 (2025) 6603-6621. https://doi.org/10.2174/0109298673304206240702062057.

[87] K. Hayashi, T. Hayashi, H. Otsuka, et al., Antiviral activity of 5,6,7-trimethoxyflavone and its potentiation of the antiherpes activity of acyclovir, The Journal of antimicrobial chemotherapy. 39 (1997) 821-824. https://doi.org/10.1093/jac/39.6.821.

[88] J.P. Kutney, H.W. Hanssen, 5,6,7-Trimethoxyflavone and 5,6,7,8-tetramethoxyflavone from Zeyhera tuberculosa, Phytochemistry. 10 (1971) 3298-3302. https://doi.org/10.1016/S0031-9422(00)97399-0.

[89] A.N. Jikah, G.I. Edo, Moringa oleifera: a valuable insight into recent advances in medicinal uses and pharmacological activities, J. Sci. Food Agric. 103 (2023) 7343-7361. https://doi.org/10.1002/jsfa.12892.

[90] N. Mara de Menezes Epifanio, L. Rykiel Iglesias Cavalcanti, K. Falcão Dos Santos, et al., Chemical characterization and in

vivo antioxidant activity of parsley (Petroselinum crispum) aqueous extract, Food Funct. 11 (2020) 5346-5356. https://doi.org/10.1039/d0fo00484g.

[91] T.A. Olasehinde, O.O. Olaokun, Apigenin and inflammation in the brain: can apigenin inhibit neuroinflammation in preclinical models?, Inflammopharmacology. 32 (2024) 3099-3108. https://doi.org/10.1007/s10787-024-01538-4.

[92] D.N. Che, J.Y. Shin, H.R. Kim, et al., Citric acid and enzyme-assisted modification of flavonoids from celery (Apium graveolens) extract and their anti-inflammatory activity in HMC-1.2 cells, J. Food Biochem. 45 (2021) e13774. https://doi.org/10.1111/jfbc.13774.

[93] W. Sun, B. Zhang, X. Yu, et al., Oroxin A from Oroxylum indicum prevents the progression from prediabetes to diabetes in streptozotocin and high-fat diet induced mice, Phytomedicine : international journal of phytotherapy and phytopharmacology. 38 (2018) 24-34. https://doi.org/10.1016/j.phymed.2017.10.003.

[94] G. Liu, W. Xie, A.D. He, et al., Antiplatelet activity of chrysin via inhibiting platelet αIIbβ3-mediated signaling pathway, Molecular nutrition & food research. 60 (2016) 1984-1993. https://doi.org/10.1002/mnfr.201500801.

[95] Y. Sun, Z. Xie, S. Shang, et al., High-efficiency UiO-66 decorated flower-like molecularly imprinted polymers for the selective enrichment of chrysin from propolis, J. Chromatogr. A. 1759 (2025) 466256. https://doi.org/10.1016/j.chroma.2025.466256.

[96] Y. Huang, C. Wang, M. Wang, et al., Oroxin B improves metabolic-associated fatty liver disease by alleviating gut microbiota dysbiosis in a high-fat diet-induced rat model, Eur. J. Pharmacol. 951 (2023) 175788. https://doi.org/10.1016/j.ejphar.2023.175788.

[97] G. Zdunić, A.A. Aradski, D. Gođevac, et al., In vitro hypoglycemic, antioxidant and antineurodegenerative activity of chokeberry (Aronia melanocarpa) leaves, Industrial Crops and Products. 148 (2020) 112328. https://doi.org/10.1016/j.indcrop.2020.112328.

[98] A. Pop, I. Fizeșan, L. Vlase, et al., Enhanced Recovery of Phenolic and Tocopherolic Compounds from Walnut (Juglans Regia L.) Male Flowers Based on Process Optimization of Ultrasonic Assisted-Extraction: Phytochemical Profile and Biological Activities, Antioxidants (Basel, Switzerland). 10 (2021) https://doi.org/10.3390/antiox10040607.

[99] B. Chi, M. Zhang, L. Sun, et al., Study on the hypotensive effect and mechanism of hawthorn (Crataegus pinnatifida) fruits and hyperoside in spontaneously hypertensive rats, Food Funct. 15 (2024) 5627-5640. https://doi.org/10.1039/d3fo02641h.

[100] L. Su, M. Zhang, Y. Zhang, et al., Transcriptome analysis reveals the crucial function of hyperoside in inhibiting anthocyanin accumulation in grape (Vitis vinifera L.) fruits by inducing VvMYB62, Frontiers in plant science. 14 (2023) 1119749. https://doi.org/10.3389/fpls.2023.1119749.

[101] I. Yoshida, M. Kumagai, M. Ide, et al., Polymethoxyflavones in black ginger (Kaempferia parviflora) regulate the expression of circadian clock genes, Journal of Functional Foods. 68 (2020) 103900. https://doi.org/10.1016/j.jff.2020.103900.

[102] W. Chen, C. Liu, X. Li, et al., 5,7-dimethoxyflavone inhibits hepatocellular carcinoma progression via increasing intestinal Akkermansia muciniphila and hepatic CD8(+) T cell infiltration, Chin. Med. 20 (2025) 170. https://doi.org/10.1186/s13020-025-01233-8.

[103] J. Yang, L. Ma, S. Di, et al., Exogenous rutin ameliorates NaCl-induced inhibition of Fagopyrum esculentum germination and early growth, BMC Plant Biol. (2025) https://doi.org/10.1186/s12870-025-08002-7.

[104] C. Zhang, X. Jia, Y. Zhao, et al., The combined effects of elevated atmospheric CO(2) and cadmium exposure on flavonoids in the leaves of Robinia pseudoacacia L. seedlings, Ecotoxicol. Environ. Saf. 210 (2021) 111878. https://doi.org/10.1016/j.ecoenv.2020.111878.

[105] Y. Li, Z. Cheng, K. Wang, et al., Procyanidin B2 and rutin in Ginkgo biloba extracts protect human retinal pigment epithelial (RPE) cells from oxidative stress by modulating Nrf2 and Erk1/2 signalling, Exp. Eye Res. 207 (2021) 108586. https://doi.org/10.1016/j.exer.2021.108586.

[106] Y. Desmiaty, N.M.D. Sandhiutami, E. Mulatsari, et al., Antioxidant and anti-inflammatory activity through inhibition of NF-κB and sEH of some citrus peel and phytoconstituent characteristics, Saudi Pharm. J. 32 (2024) 101959. https://doi.org/10.1016/j.jsps.2024.101959.

[107] F. Cáceres, J. Vallès, A. Gras, Exploring Ethnobotany in the Catalan Linguistic Area: Traditional Plant-Based Knowledge for Addressing Gastrointestinal, Metabolic, and Nutritional Disorders, Plants (Basel, Switzerland). 13 (2024) https://doi.org/10.3390/plants13172453.

[108] J. Stabrauskiene, M. Marksa, L. Ivanauskas, et al., Optimization of Naringin and Naringenin Extraction from Citrus × paradisi L. Using Hydrolysis and Excipients as Adsorbent, Pharmaceutics. 14 (2022) https://doi.org/10.3390/pharmaceutics14050890.

[109] N.M. Ammar, H.A. Hassan, H.M.I. Abdallah, et al., Protective Effects of Naringenin from Citrus sinensis (var. Valencia) Peels against CCl(4)-Induced Hepatic and Renal Injuries in Rats Assessed by Metabolomics, Histological and Biochemical Analyses, Nutrients. 14 (2022) https://doi.org/10.3390/nu14040841.

[110] M. Milićević, A. Isa, S. Yayla, et al., Nanocomposite enhanced molecularly imprinted polymer for electrochemical detection of naringenin in plant-based samples, Mikrochimica acta. 192 (2025) 642. https://doi.org/10.1007/s00604-025-07489-z.

[111]B.A. Lone, N. Sharma, D. Kour, et al., In-vitro anti-sickling potential of baicalin and naringenin isolated from Oroxylum indicum and Citrus aurantium on human sickle red blood cells, Nat. Prod. Res. 37 (2023) 3902-3908. https://doi.org/10.1080/14786419.2022.2158330.

[112] M.G. Campos, R.F. Webby, K.R. Markham, The unique occurrence of the flavone aglycone tricetin in Myrtaceae pollen, Z. Naturforsch. [C]. 57 (2002) 944-946. https://doi.org/10.1515/znc-2002-9-1031.